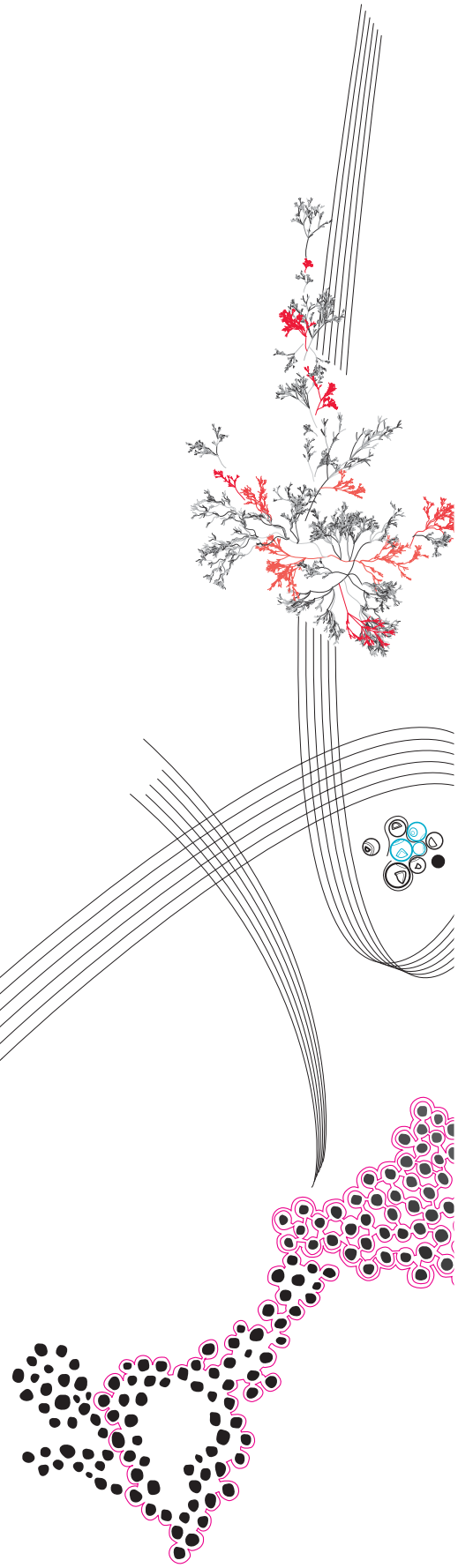

Master Thesis

Rate-Dependent Properties and Failure Behaviour of Glass Fiber Reinforced Isotactic Polypropylene Composite Laminates under Impact Conditions

Roy van Zijl

EXAMINATION COMMITTEE
Dr. Ir. T.C. Bor
Dr. I Baran
S. Aktas, MSc
Dr. M.I. Abdul Rasheed

September 21, 2021

DOCUMENT NUMBER
MS3/PT-0080

Faculty of Engineering Technology
Department of Design, Production and Management

UNIVERSITY OF TWENTE.

Summary

Passenger cars are an important part of personal transport. Due to their popularity, they have a significant influence on climate change. One of the main factors influencing fuel consumption and emission levels is the total mass of the vehicle. Using fiber reinforced thermoplastic composites can be a solution to this problem. Their low density and high strength can lead to lighter cars without neglecting safety measurements. Safety is an important aspect in transport as accidents with injuries or possible fatalities occur often.

Cars are designed in a way that the structure and material is capable of absorbing impact energy during a collision or accident. A material is capable of absorbing energy by deforming and via the introduction of failure modes. For common structural materials such as steel or aluminum, this energy absorbing process has been subject of many research projects. As a result, the energy absorbing capability of these materials as well as the failure behavior can be predicted via models. This is as of yet not possible for thermoplastic composites.

It is known that the material properties and failure behavior of composite materials are dependent on the strain rate. Extensive experimental research has been performed on the effect of strain rate on the tensile properties of composite materials. However, these do not give a full overview of how the material responds in the case of a low velocity impact situation. It is therefore required to acquire data on the response behavior of these materials under impact loading in order to develop predictive models which can be used for designing the composite structures.

In this work, an experimental testing procedure was set-up to investigate the relation between the strain rate and material properties and failure behavior of a glass fiber reinforced isotactic polypropylene in impact situations. This was done by quasi-static three point bending testing and low velocity drop weight impact testing. Three point bending tests at lowered temperatures were carried out to investigate the influence of temperature on the material properties and failure behavior as well as discussing the possibility of using the time-temperature-superposition principle to mimic higher strain rates.

Results showed that the fiber orientation has a large influence on the material properties of the composite, independent of the used research method and strain rate. 0° specimens showed moduli which were up to 6 times higher, a flexural strength up to 20 times higher and a strain at failure of 2 to 8 times higher than in 90 degree specimens.

An increase in strain rate led to an increase in flexural strength, energy absorption and strain at failure for nearly all experiments. The modulus proved to be rate-independent, but highly temperature dependent for 90 degree specimens.

Matrix cracking was the only failure mode found in 90 degree specimens. The amount of absorbed energy was directly proportional to the crack depth. 0 Degree specimens showed matrix cracking and fiber fracture at all experiments, if a lower threshold of energy being put in to the specimens was achieved. At higher energy levels, larger areas were affected by these failure modes and delaminations were found. Once again, the area affected by these was proportional to the absorbed energy. An upper limit to this energy absorption was also found.

The used research methods are difficult to directly compare as the low velocity impact tests yielded

much lower absolute values. Furthermore, the influence of the temperature on the material properties itself was larger than the influence of the strain rate. For 0° specimens, it is possible to use lower temperature quasi-static testing to achieve higher strain rates. This is not possible for 90° specimens.

To fully understand and predict the rate-dependency of failure behavior of thermoplastic composites, more research is required, especially when taking into account the influence of material thickness, lay-up and structural shape of the specimens. The aforementioned time-temperature-superposition can be used in certain cases, albeit with some care. Correlating these results with tensile, shear and compression testing is also required for the creation of a predictive model for the short-term behavior of thermoplastic composites.

Preface

Finishing this thesis also marks the end of a very interesting period consisting of low lows and high ups. As a fanatic athlete, my only goal was to do better than I have ever done before. Knowing that this thesis has some of my best work in it makes me proud. And yes, there are some sections which could have been better, and there are some things that did not go as smoothly as they were supposed to, but there is always room for improvement. This marks the end of my 6 year long career as a student here at the University of Twente, fortunately I'm able to pursue my career here in a PDEng program.

I could not have finished this thesis by myself. I would like to thank my supervisors, Senem Aktas and Ismet Baran for their support over the last 11 months. They have provided me with lots of knowledge and insight, as well as some good laughs here and there. Even with my busy non-academic schedule, there was always a way of helping me out and finishing this project.

I would also like to say a massive thanks to my parents and sister, who have provided me with plenty of love and mental support when needed. This also applies to my friends, who have been there whenever I needed them.

Contents

Chapter 1

Problem Definition

Cars are one of the most common forms of personal transport. In the Netherlands alone, there were 8.678 million passenger cars as of January 2020. Out of these vehicles, 402.000 were either fully electrical or hybrid [16]. Passenger cars have an considerable environmental impact due to their CO_2 emissions and fossil fuel usage.

With new regulations and limitations on the allowed emissions and fuel usage, car makers are looking for ways to improve their vehicle design. Most brands now offer a wide variety of hybrid or full electric models which meet these new regulations. A number of hydrogen powered cars are also on offer at the moment. Car makers have also limited the emissions and fuel consumption of their vehicles by fitting them with smaller, turbocharged engines running on conventional fossil fuels.

It is clear that decreasing fuel usage is of great importance. Friedrich and Almajid [28] estimate that 75% of a vehicle's fuel consumption is directly related to its weight. With everything else remaining the same and considering mass compounding, a 6 - 8% increase in fuel economy can be realised for every 10% reduction in weight.

Due to the ever increasing customer desire for luxury in both equipment and space, vehicle size has increased a lot over the years. These luxury levels also directly impact the vehicle weight. It must however be noted that the largest increment of size is done based on more severe safety requirements.

With the large number of vehicles present, a similar large number of accidents can be expected. In 2019, 73.265 accidents involving at least 1 passenger car occurred in the Netherlands. Out of these, 10.823 led to any form of injury to one of the drivers or passengers with a further 348 leading to at least one fatality (not necessarily within the passenger car) [56]. In total, 237 people died as driver or passenger within a passenger car in the Netherlands in 2019.

Given that the amount of incidents concerning passenger cars - which resulted in either injury or fatality - has dropped by 50% in the last 30 years, it is clear that the stricter safety requirements have paid off [56].

In order to lower fuel consumption and emissions even further whilst not compromising in the luxury and safety department, solutions other than those based on the drive train have to be found. This can be done in the form of using different materials for both the structural cell as the bodywork of the passenger car [11]. Currently, most passenger cars are constructed using aluminum, steel or a combination thereof. Aluminum in itself has a lower density than the steel, which makes it suitable for weight reduction. Steel on the other hand is stronger so less material is required to achieve an equal level of stiffness and structural strength.

With the current progressions in material technology, a third option has arisen; the use of composite materials. These materials combine the strength and stiffness of fibers with the flexibility and low density of a polymer matrix. The overall advantages of using composites when compared with steel in passenger cars are: (1) weight reduction of 20–40%; (2) styling flexibility in terms of deep drawn panels,

which is a limitation in metal stamping; (3) 40%–60% reduced tooling cost; (4) reduced assembly cost and time in part consolidation; (5) resistance to corrosion, scratches, dents, reduced noise vibration harshness and higher damping; (6) materials and process innovations capable of adding value while providing cost savings; and (7) safer structures due to higher specific energy absorption [28, 43].

Especially the latter advantage mentioned above is of interest. Composite materials tend to have a brittle fracture behavior. This fracture behavior means that at impact, the material will shatter without elastic or plastic deformation. These types of deformation are however responsible for a lot of energy absorption during impact. It is therefore of great importance to design structures made out of composite material in such a way that the load is transmitted from the point of impact further into the structure, as proposed by Savage et al. [51].

The impact and crushing behavior of a composite material is, besides brittle, extremely complex. It also consists of several damage modes due to the combination of fibers and matrix materials [26]. This behavior is therefore complex to predict which makes it difficult to use these materials in applications where the risk of impact or crushing is present, which is the case in passenger cars.

A large variety of composite materials is available due to the wide range of possible combinations of matrix and fiber materials. These can be categorized based on two main criteria; the type of matrix material and the length of the fibers used. The length of the fibers used can be either short or continuous whereas the type of matrix material is either thermoset or thermoplastic.

Continuous fiber reinforced thermoset composites are most commonly used in cars. They are mostly found in high-end road cars or race cars, which all use the weight reduction for increased performance. Weight reduction for the sake of improved fuel consumption or emission reduction is still rare. However, due to advancements in production technology, the possibility of using continuous fiber reinforced thermoplastic composite materials is rising. This is advantageous as thermoplastic composite materials can be manufactured more cheaply than thermosets. Furthermore, one of the great advantages of thermoplastic composites over thermoset ones is their ability to be recycled [11]. Especially in times were recyclability is such an important topic, this is of great interest for manufacturers.

The use of continuous fiber reinforced thermoplastic composites is therefore desirable for passenger car manufacturers. It has a large number of advantages over conventional materials and can be used for both structural and bodywork purposes. The major drawback is the complex damage behavior which is also difficult to predict. Due to the large number of (severe) accidents with passenger cars, safety remains the highest priority. Understanding this behavior and stating design guidelines for its use is therefore of great importance.

For common structural materials such as steel and aluminum, predictive models for the material behavior under impact conditions exists. This is as of yet not the case for thermoplastic composites. In addition to the already complex failure behavior of composites, their material properties and failure behavior is strain rate dependent. This means that the behavior is dependent on the rate of deformation which is applied to it. Especially when used in passenger cars, a wide range of impact velocities - and therefore deformation rates - is present. This adds an extra layer to the importance of predicting the failure behavior for short term deformations.

Chapter 2

Research Questions

The problem definition leads to one very important statement: the predictability of the failure behavior of thermoplastic composites on very short term impact situations. A number of subjects to study can be defined from this statement. Firstly, the failure behavior of thermoplastic composites should be investigated. This behavior is complex and can consist of a number of so-called failure modes. These failure modes are ways of absorbing energy. Understanding the relation between the different failure modes and their energy absorbing capability is of great interest. This connection is very useful when creating a failure model of the material.

There is a wide variety of thermoplastic composites available. Even beyond the material selection, a large number of variables which highly influence the material properties and failure behavior are present. Identifying their influence is also of great value. Finally, the mentioned strain rate dependency is a key part of the research to be done. A large dependency on the strain rate will alter the usability of a material.

2.1 Damage

The resulting damage is also dependent on the type of crash that occurs. There are however multiple very important variables which determine the damage resulting from a crash/an impact. These are listed below:

- **The velocity at which the crash occurs**. This is of importance for all types of crashes. In the case of a multi vehicle crash, it is important to look at the impact velocities of all vehicles with respect to each other. The impact velocity has a 60% influence on the extent of injuries sustained in crashes [60], and it is assumed that this influence is similar for material damage.
- **The part of the passenger car where the impact is located**. Safety measures are strict for the entire vehicle, but more impact prone regions exist which should be further reinforced. Furthermore, this has a large influence on the risk of injury for the passengers. Zeng et al. have produced a Point of Interest list consisting of 21 different zones of a passenger car with corresponding levels of risk of injury for the passengers [68].
- **The angle and offset at which the impact occurs**. The angle at which the impact occurs implies the angle between the direction of the passenger car velocity and that of the impact object(s velocity). The offset is somewhat related to the impact location as it is based on the distance from the center of gravity of the passenger car. Both these factors have about a 20% influence on the extent of injuries sustained in crashes [60]. Examples of these include head-tail, sideswipe or frontal collisions in multi-vehicle accidents [17].
- **The material and geometry used at the impact location**. Each material has a different specific energy absorption which means that crashes with similar energies cause different grades

of damage, based on the material. Since the material will be the main investigated variable, it will be further evaluated later. This also applies to the geometry.

Based on the results found in the previous paragraphs, it can be concluded that there are plenty of variables responsible for the damage outcome of a passenger car crash. Since this thesis is time restricted - it is impossible to predict the damage for every crash scenario - a selection will be made based on the risk of a certain type of crash. The risk in this case is the relation between the crash occurrence and its severity. Herein, the crash severity is based on the chance of injury for the passengers of the car.

The most important parameter for the further analysis of the damage prediction is the impact energy. This parameter is based on nearly all variables mentioned in the previous paragraphs, excluding the material and geometry used at the impact location, and is proven to be extremely useful in damage prediction [1, 26, 59]. There are multiple ways of calculating the impact energy presented in literature (i.e. by Zeleniakiene et al. [67]) but as of yet there has not been found a research dedicated to relating the impact energy to a specific crash situation.

2.2 Translation to Experimental Data

A lot of research has been done on the impact properties of continuous fiber reinforced thermoplastic composites [2, 5, 9, 12, 37, 39, 53, 54, 65]. This research was based on so-called 'low velocity' impacts executed with a drop-weight. Most research is done at velocities < 10 m/s, which is seen as the standard below impact situations are called low velocity [47], which is far below the average speed at which passenger car accidents occur [56].

These experiments also took place with small impactors with diameters around 10 - 20 mm and a weight of around 5 - 10 kg. It can be easily imagined that most car crash situations will involve much larger objects. It has to be noted that the used specimens have dimensions of around 150 x 150 mm, which is an important ratio to compare crash situations to the experimental data.

Falzon et al. [25] did tests on a survival cell structure at similar low velocities (10 m/s) while using a sled weight of 780 kg and drop weights of 26 kg, which has a huge influence on the impact energies. Basith et al. [7] did tests with 3D models of a car bumper at average crash velocities (40 - 80 km/h or 11 - 22 m/s). These results may therefore be more representative of the expected results in real life crash situations.

It has to be noted that the goal is to recreate the damage that will result from a crash at smaller scale in order to save costs as current iterative crash tests are expensive [25]. The resulting damage profile and material properties can then be used to validate models to predict the behavior of the material during crashes. In the end, the creation and validation of these models is the most important research goal within this thesis.

The rate-dependency of polymers and fiber materials has also been subject of study in a lot of research work [3, 21, 29, 30, 45, 52, 63]. However, nearly all of these were performed under tensile testing conditions. Tensile properties, although extremely common and useful when making design choices, do not fully represent the material behavior under impact conditions. It can be easily imagined that the effects of compression and flexion due to bending are different than those caused by tension.

One of the few papers combining tensile and flexural testing is that of Bledzki et al. [10]. Herein, a number of hybrid composites (including bio-composites) are evaluated using tensile and three point bending testing. Their work shows a significant difference between the two testing methods. This further underlines the need to use flexural testing.

2.3 Novelties

In order to properly relate the influence of strain rate on the material properties and failure behavior of a thermoplastic composite, the need for a wide range of strain rates is required. It is hereby important to replicate the other testing parameters as much as possible. This leads to the combination of low velocity impact testing using a drop weight impact tower and high strain rate quasi static three point bending testing. The idea of combining three point bending test with a drop weight impact tower was first proposed by Lobo and Lorenzo [42] and further evaluated by Lobo and Barthelat [6] for material properties and Jacob et al. [34] for energy absorption.

This ideology was used as a baseline for a part of this thesis. The relations between the fiber direction, strain rate and testing set-up and the material properties and failure modes of a thermoplastic composite are investigated in this thesis. To the fairest of the authors knowledge, this is the first work to combine these research methods into the material properties and failure behavior of thermoplastic composites. Furthermore, it is accompanied by an optical investigation into the failure modes and their energy absorbing capabilities.

The research goals for the entire project are listed below. Due to their complexity and the limited time available for this thesis, there may not be fully conclusive answers to all of the goals.

Main Research Goal

Develop a predictive model for the short term behavior of thermoplastic composite, find experimental data to validate the predictive models

1st Research Goal

Identify the influence of fiber direction on the material properties and failure behavior

2nd Research Goal

Identify the relation between the strain rate and the stiffness, strength and strain at failure of thermoplastic composites under impact loading

3rd Research Goal

Identify the failure modes of thermoplastic composites under impact loading

4th Research Goal

Correlate the low velocity impact testing with high strain rate quasi-static bending

Chapter 3

Methodology

In order to achieve the research goal set in section 2, a number of steps have to be taken. These include the gathering of data from previously done research and checking it with experimental data acquired from testing.

3.1 Literature Research

The literature research - section 4 - focuses on the discovery of suitable research methods for the experimental research. Furthermore, it is key to discover the important properties to be investigated, along with the range wherein the results can be expected. It is also important to find relevant research to fundamentally argue the need for this research to be done. It can also be concluded that it is important to rule out that this specific research has already been done.

In the case of a material property research, it is important to find already executed research with respect to similar materials. In this case, the research is focused on a glass fiber filled thermoplastic composite. Even though there can be major differences in the absolute material properties, there can be some important relations that occur throughout the entire material group, as proven by Nurul Fazita et al. [44].

3.2 Material

Throughout all experimental processes, pre-fabricated sheets are used. These are made using UD-MAX™ GPP 45-70 Tape, which is a prepreg with continuous glass reinforced isotactic polypropylene matrix. The prepreg has 45% and 70% fiber volume and fiber weight fractions, respectively. The tape has a width of 110 mm and thickness of 0.25 mm. Resin's melting temperature is 163° C. The plates manufactured consist of 8 layers, with a total thickness of 2 mm.

Laminates were heated to 220 °C (consolidation temperature) . During heating, a low pressure is applied to ensure contact between the plates of the press and the mold for heat transfer (a pressure of 1 bar is about the lowest controlled pressure that can be applied using the 390*390 mold, which corresponds to about 14 kN). The mold was kept at consolidation temperature for 10 minutes and then cooled to room temperature. From 220° C to 200° C, air cooling is used. From 200° C down to room temperature, water cooling is used at its full capacity, that is to say, valve fully open(4.4-5 K/min).

The sheets consists of a single fiber direction (0°) and are cut with a diamond circular saw in such a way that when tested, 0° and 90° specimens are created. The rectangular specimens have dimensions of 60 x 12 x 2 mm, given some production margins. All specimens are polished after cutting. All specimen data can be found in the table in appendix A.

3.3 Quasi-Static Testing

Firstly, it is useful to understand the material behaviour at quasi-static strain rates. As the name already mentioned, it involves low strain rates which near a static state (0 s^{-1}). The main goal of quasi-static testing is the determination of material properties themselves. It can also be used during fatigue testing wherein a low strain rate is applied for a long period of time to represent use.

Quasi-static testing can be done in a number of different ways. The main categories are tensile, bending, compression and shear testing. Tensile testing is based on the elongation of the material and its resistance thereof. This will lead to material properties such as the Young's Modulus. Bending testing is usually done via a three point bending (3PB) test. Herein, the material specimen is laid upon two supports and a force/load is applied in between, thus creating the three points. From these tests, flexural properties can be determined. The flexural modulus however is equal to the Young's modulus in the case of an homogeneous material [4]. Compression testing is used for looking at the compressing abilities and resistance of the material. This is mostly executed by applying a force/load onto the entire specimen, thus crushing it from the top. For crash testing, this is quite important. Finally, the shear resistance of the material is based on shear forces and stresses.

Due to the major influence of the fibers and their direction on the material properties, the results of these different types of testing can differ enormously. Their importance is therewith reinforced.

The quasi-static testing is executed via a three point bending (3PB) test. This test is done via the ASTM D7264M standard for the testing of the flexural properties of polymer matrix composites. In this test, a specimen is laid upon two supporting points, with an equal distance between the edge of the specimen and the supporting point on either side. A load is applied in the middle of these supporting points - by moving the supporting points upward while keeping the loading point stationary -, such that the distance between the edge of the loading point and the supporting point is equal on either side.

The specimens used have dimensions of 60 x 12 x 2 mm. All tests are done for both specimens with fibers in the transverse direction (parallel to the loading point), as well as those with fibers in the unidirectional direction (perpendicular to the loading point). The supports were placed 43 mm apart, and have a radius of 2 mm. The impactor has a radius of 5 mm. A Roell-Zwick machine was used with a force cell capable of 5 kN. The test-setup is shown in figure 3.1. As mentioned before, the bending speed (crosshead speed) is varied as it is the main research criterion. For room temperature testing, the crosshead speed is set to either 2, 20 or 200 mm/min. The program is stopped when a force drop of 30% is noticed or when the absolute displacement (as measured by the crosshead) reaches 5 mm.

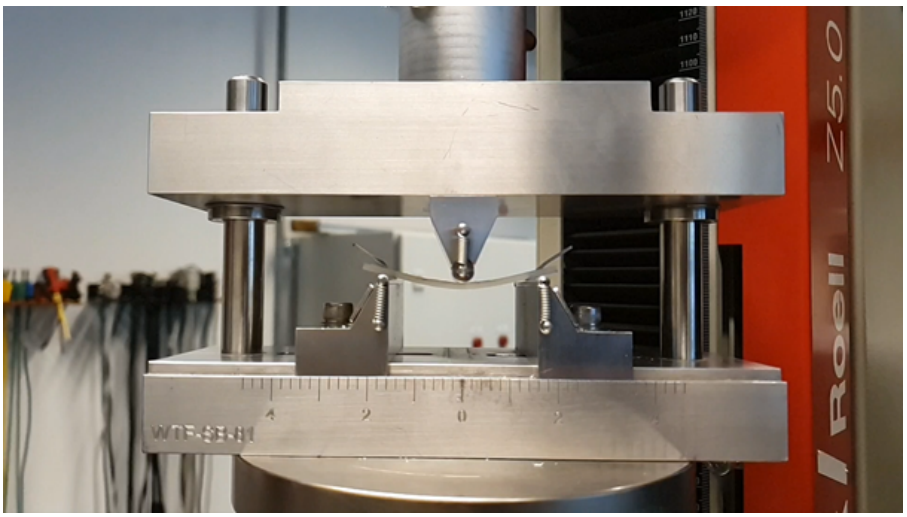

Figure 3.1: Set-Up of the 3 Point Bending Quasi Static Tests

The resulting force, time and displacement data as well as the specimens themselves are used for

further evaluation. These force-displacement curves can give vital information about the material behaviour of the specimens. This is mainly focused on the moment of failure as well as the built-up to it. Often, this curve starts out close to linear, after which the material will pass a so-called yield point. After this point, there will be a very small increase in stress before failing. The material will actually already fail at the yield point, but some of the cracks or crazes within it will still be able to resist some stress. A decrease in stiffness is however directly noticeable.

If a material is brittle, it will fail very shortly after reaching this yield point. This means that after the yield point is reached, a small 'hat' to the graph can be seen, which consists of a slight increase in force for a small displacement before it decreases with even further displacement until failure. A ductile material will also show this 'hat' shape, but will be able to deform much further (at this lower force level) before finally failing [61].

Similar to the force-displacement curve, a stress-strain curve can be found. This curve looks similar to the previously mentioned force-displacement curve, albeit with an independence on the properties of the tested specimens. In order to calculate the flexural strain, equation 3.1 was used. In this equation, D stands for the maximum deflection. In this case, that will be the displacement at time of peak force (as seen in table 5.1). The d stands for the thickness of the specimens used, this can be found in tables A.1 and A.4 in appendix A. Finally, the L stands for the span length, which has been set to 43 mm, as mentioned in the introduction of this section.

$$\epsilon_f = \frac{6Dd}{L^2} \tag{3.1}$$

The flexural modulus can be determined by looking at the slope of the force-displacement curve. Since the material has a non-linear force displacement behavior (especially near failure), it is important to take a look at the linear part of the curve. This is done by using the part between 10 and 50% of the force at failure. The actual calculation is given by equation 3.2, as proposed by the STP674 standard [69]. In this equation, the aforementioned slope is denoted by m. The other parameters have been mentioned before; the span length is denoted by L, as well as the specimen width (b) and thickness (d).

$$E_{flex} = \frac{L^3 m}{4bd^3} \tag{3.2}$$

In order to calculate the absolute strength (or bending stress at failure), equation 3.3 was used. In this equation, F stands for the peak force as shown in table 5.1. L_0 stands for the length of the used specimens, which is set to 60 mm, as mentioned in the introduction to this section. The d stands for the thickness of the specimens used and the b for its width, the values for the used specimens can be found in tables A.1 and A.4 in appendix A.

$$\sigma_b = F\frac{L_0}{4}\frac{\frac{d}{2}}{\frac{bd^3}{12}} \tag{3.3}$$

Finally, an important aspect of this research is the energy absorbing capability of a material. The total amount of energy absorbed is defined as the area under the force displacement curve. This can be calculated by integrating the force with respect to the displacement, as can be seen in equation 3.4 [34]. In this equation, E_{abs} represents the total amount of absorbed energy, F the measured force, S the measured displacement and S_b the final deformation. In order to calculate the so-called specific energy absorption (energy absorption per unit mass), W is simply divided by the total mass of the specimen.

$$W = \int_0^{S_b} F dS \tag{3.4}$$

The quasi-static three point bending tests are to be executed at three different crosshead velocities: 2, 20 and 200 mm/min. Measurements start when a force of 5 N is measured. Up unto this point, the crosshead speed (used to determine the modulus by the machine itself) is 5 mm/min. Tests are aborted when a 80% force drop is measured.

3.4 Low Velocity Impact Testing

Especially for crash testing, the material behaviour at and after impact is useful to investigate. However, due to the expensive testing procedures required for impact testing, a low-velocity impact test is used. This test can be done by using a weight which is dropped from a height onto the specimen. The test can also be executed by using an impact pendulum which impacts the specimens from the side.

Low Velocity Impact testing causes higher strain rates within the material due to the impact velocity of the impactor. It can be classified as medium strain rate testing. One of the most important parameters to change during impact testing is the impact energy, as discussed in section 4.4. This can be done by either altering the mass, in the case of a drop weight impact test, or the impact velocity. The latter one can be done by changing the height of the drop in a drop test, or the height of the pendulum in a side impact test. Using a combination of these two changes, different energy levels can be achieved.

Besides changing the energy levels of the impactor, it is possible to influence the strain rate achieved within the material using these tests. This is due to the relation between the strain rate and the velocity of the impactor. Due to an energy transition between the impactor, the specimen and the surrounding, this is not a perfect velocity transfer. It is therefore difficult to predict the actual strain rate within the material before the tests are done.

Materials used in automotive industries are in high risk of being involved in an impact type situation. Impact in itself is defined as the (forceful) contact between at least two bodies, as also explained in section 4.4. During studies, impact situations are often distinguished by their short duration. In other words, an impact event will cause an energy transfer within a very short period of time. Since nearly all forms of energy transfer in material science involve the deformation of at least one of the two bodies, the strain rate (deformation per unit time) will be high.

In order to investigate the effect of this higher strain rate on the material properties and behavior, low velocity impact tests are executed (as explained in section 3.4). Testing was done on a Dynatup 8250 Falling Weight Impact Machine. In order to achieve results which can be easily compared to the quasi-static cases, a set-up was designed to mimic the circumstances of the quasi-static tests.

This set-up, as shown in figure 3.2 consists of two supporting cylinders, with a radius of 2 mm. Although it might not be very clear from the figure, the specimen itself can only make contact with these cylinders and not with the material behind it. In earlier iterations, the specimens were clamped at both ends. This however resulted in the presence of three different and unwanted failure zones: one at the point of impact and the other two at the supporting cylinders. For the sake of comparability to the quasi static experiments, the clamps were removed. Similar to the quasi-static case, a span of 43 mm between the supporting cylinders - with a radius of 2 mm - was used. The impactor was fitted with a cylindrical tup with a radius of 5 mm. The system itself is equipped with an oscilloscope based data acquisition system.

For the general investigation into the acquired results, the work of Barthelat and Lobo [6] is used. Their work is also based on the general idea of comparing the results of quasi static three point bending testing and low velocity impact testing using a drop weight impact machine. This direct comparison is however not as straightforward, as the energy transfer between the impactor and specimen is not as ideal as during quasi static testing. Factors that influence this energy transfer include the rebounding of the impactor after impact, friction during the drop phase and the introduction of kinetic energy to the specimen (i.e., giving a velocity to the specimen). Given these conditions, a 100% energy transfer

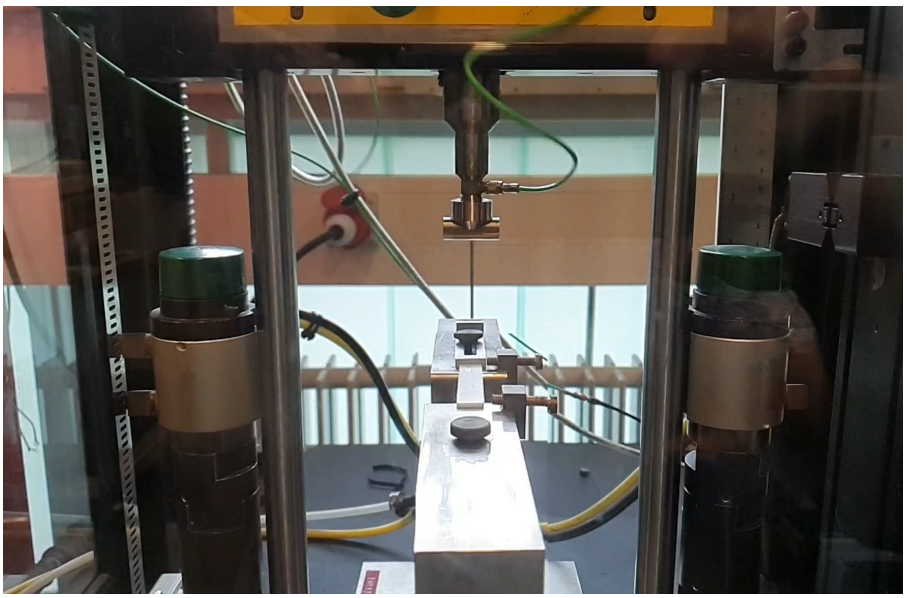

Figure 3.2: Set-Up of the Low Velocity Impact Tests

between the impactor and specimen will not happen. This implies that the penetration zone of the Energy Profiling Method of Aktas et al. [1] (see section 4.5.2) can never be reached with this set-up.

Since the load cell is responsible for the collection of data, it is important to understand where this data comes from and how it can be used. Equation 3.5 [6] shows the standard formulation of the force levels within the crosshead. In this equation, m represents the mass of the crosshead, the load cell and the cylindrical tup (using the total mass in stead of the crosshead mass as proposed by Barthelat and Lobo [6] removes the discussion about the inertia of the loading nose), $a(t)$ its acceleration, g the gravitational constant and $F(t)$ the force.

$$ma(t) = mg - F(t) \tag{3.5}$$

In order to express the velocity of the crosshead ($v(t)$), a single integration is required. This result, which includes v_0 as the velocity at the starting point - specified by the drop height h -, is shown in equation 3.6.

$$v(t) = v_0 + gt - \frac{1}{m}\int_0^t F(t)dt \tag{3.6}$$

Since the force-displacement curve is of great interest, it is of importance to express the displacement $x(t)$ of the crosshead. Removing the initial drop height h from this value will lead to the final deformation d of the centerpoint of the specimen. Equation 3.7 shows the relation between the displacement, measured force and measured time. It is found by once again integrating equation 3.6.

$$x(t) = v_0 t + \frac{1}{2}gt^2 - \frac{1}{m}\int\int_0^t F(t)dt \tag{3.7}$$

These equations have been implemented in the ImpactLogger software - of which version 2.2 was used during the experimental phase - designed by Warnet. Furthermore, an external position sensor is added to the system to verify the calculations. This position sensor is based on a light sensor and a rod filled with holes each representing a step of 0.2 mm. The resulting displacement will therefore only be measured in steps of 0.2 mm and is therefore more of a step function than a smooth curve. A further analysis of the results will require the calculation of the stress and strain within the material.

Again, Barthelat and Lobo have formulated these equations for small deformation in the outer fibers [6].

The engineering strain is given by equation 3.8. Herein, ϵ represents the strain at the outermost fiber, t the thickness of the specimen, d the aforementioned displacement at the center of the specimen and L the span length. The strain rate (strain function once differentiated by time) is given by equation 3.9. Herein, $\dot{\epsilon}$ is the strain rate at the outermost fiber and v the velocity in the center of the beam.

$$\epsilon = 6\frac{td}{L^2} \tag{3.8}$$

$$\dot{\epsilon} = 6\frac{tv}{L^2} \tag{3.9}$$

For the calculation of the stress at the outer fiber, two different options depending on the assumption of the stress profile within the specimen are available. A linear elastic stress profile, as seen in figure 5.18a, will lead to equation 3.10. If perfect and total plastic deformation at yield (stress profile seen in figure 5.18b) is assumed, the stress can be calculated using equation 3.11, as denoted by Trantina and Oehler [58]. In both cases, F stands for the measured force, L for the span length, w for the specimen width and t for the specimen thickness.

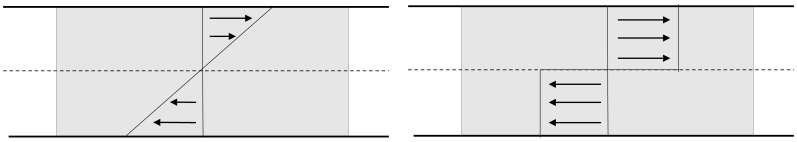

(a) Linear Elastic (b) Totally Plastic

Figure 3.3: Stress profiles for beam in flexion

$$\sigma = \frac{3}{2}\frac{FL}{wt^2} \tag{3.10}$$

$$\sigma = \frac{FL}{wt^2} \tag{3.11}$$

Provisional results during the test phase of the test set-up itself showed a total plastic failure behavior of the specimens. Therefore, it was decided to assume the presence of a total plastic stress profile and to use equation 3.11 for the stress calculations.

Testing itself was based on two different scenarios: finding the relation between material properties and failure behavior and the applied impact energy (scenario I) and strain rate (scenario II). This was also done by Boria et al [12]. A starting drop height h was determined by using the smallest drop height possible for the testing rig, along with an accompanying mass - in the first case just the holder of the crosshead, the impact tup and load cell - after which its maximal impact energy was determined. It has to be noted that this is the impact energy in an ideal scenario as there is friction between the guiding rods and crosshead in play during the drop. A second testing phase was to be executed with double the impact velocity of the first phase, which meant a quadrupling of the impact height for the same mass. Again, this is based on the ideal scenario, since a larger drop height will most likely cause more friction and thus a lower real impact energy.

For the 90° specimens, these first two test set-ups proved to be functional as the specimens already showed complete failure at these energy levels. The set-ups are shown in table 3.1.

Provisional testing with the 0° specimens led to the conclusion that a higher amount of impact energy was required to cause any noticeable damage. It was therefore chosen to add mass plates to the drop weight impact machine and recalculate the drop heights for these specimens. Due to physical limits of

Table 3.1: Test-set up of Low Velocity Impact tests for 90° specimens

Drop height [mm]	Mass [kg]	Max Impact Energy [J]	Max Impact Velocity [m/s]
15	1.588	0.2336	0.5424
60	1.588	0.9347	1.0850

the testing rig, the final step is reduced to 150% of the previous step, in stead of the previously used doubling. The highest impact energy value of the 90° specimen tests was used as a guideline for these calculations, as seen in table 3.2.

Table 3.2: Test-set up of Low Velocity Impact tests for 0° specimens

Drop height [mm]	Mass [kg]	Max Impact Energy [J]	Max Impact Velocity [m/s]
18.5	5.114	0.9281	0.6025
74.4	5.114	3.7325	1.2082
297.4	5.114	14.9201	2.4156
892.4	5.114	44.7702	4.1844

As mentioned before, two different scenarios were to be investigated. During testing of the second scenario (effect on the strain rate itself) some errors occurred which led to the acquired data being not usable for this thesis. The effect of the strain rate itself was to be measured by replicating the same level of impact energy (ideal/maximal level, as theoretically calculated) with different set-ups of drop height and drop weight. This would lead to testing results executed at the same energy level but with different impact velocities. Any noticeable differences between these results would therefore imply a material property relation with the strain rate itself, not just the impact energy. This was also investigated for PP tape by Boria et al. [12] and for PEEK composite materials by Vieille et al. [62].

3.5 Low Temperature Quasi-Static Testing

The use of composite materials in cars brings some more challenges than just the difference in material behavior at different strain rates. The influence of temperature on the material behavior is also important. Especially at lower temperatures, composite material can show extremely brittle behavior. Since passenger cars are used globally, it is very likely that the material will encounter temperatures below 0 Celsius. In most cases, this is close to the glass-transition temperature of the polymer used in the composite. Identifying the influence of the temperature on the material behavior is therefore of great importance.

The test set-up used is equal to that of the quasi static 3 point bending tests. This includes the radii of the supports and impactor, as well as the dimensions of the samples and the span between the supports. These values can be found in section 3.3. Testing was executed at a bending speed of 20 mm/min at room temperature - in order to facilitate comparison - and at 3 different temperature levels: 0, -15 and -30° Celsius (273, 258 and 243 K).

It is possible to mimick higher strain rates at lower temperatures or lower strain rates at higher temperatures (such as creep, as done by Erartsin et al. [24]) by applying the Time-Temperature-Superposition principle as proposed by Govaert and Van der Vegt [61]. Although not a part of this thesis, the data acquired in the temperature dependent testing can be used as a starting point to implement this. A further explanation and guideline for this is given in section 7.

3.5.1 Visual Analysis

In order to fully understand what is happening within the material, a visual investigation is necessary. This is done via optical microscopy and scanning electron microscopy (SEM). Due to the large variety of possible failure modes, it is of great importance to understand which failure modes occur at different

strain rates. Furthermore, the affected area is of importance as it is a large factor in determining the amount of energy that is absorbed by said failure mode.

The optical microscopic analysis is done using a Keyence VHX-7000 Digital Microscope. Firstly, the specimens are cut to size using a diamond bladed circular saw. The cut specimens are then placed into a holder before being submerged into an epoxy bath. Hardening leads to the specimens being embedded into the clear epoxy. The finished samples are then polished before being inspected with the microscope.

It is of great importance to identify the different failure modes during inspection. A list of the possible failure modes is given in section 4.2. Figure 3.4 shows one of the provisional specimens, along with some detailed looks at common failure modes. Some of the failure modes cannot be completely shown by optical microscopy, the most important one of these is fiber pull-out. This is only visible with the naked eye or when using a SEM.

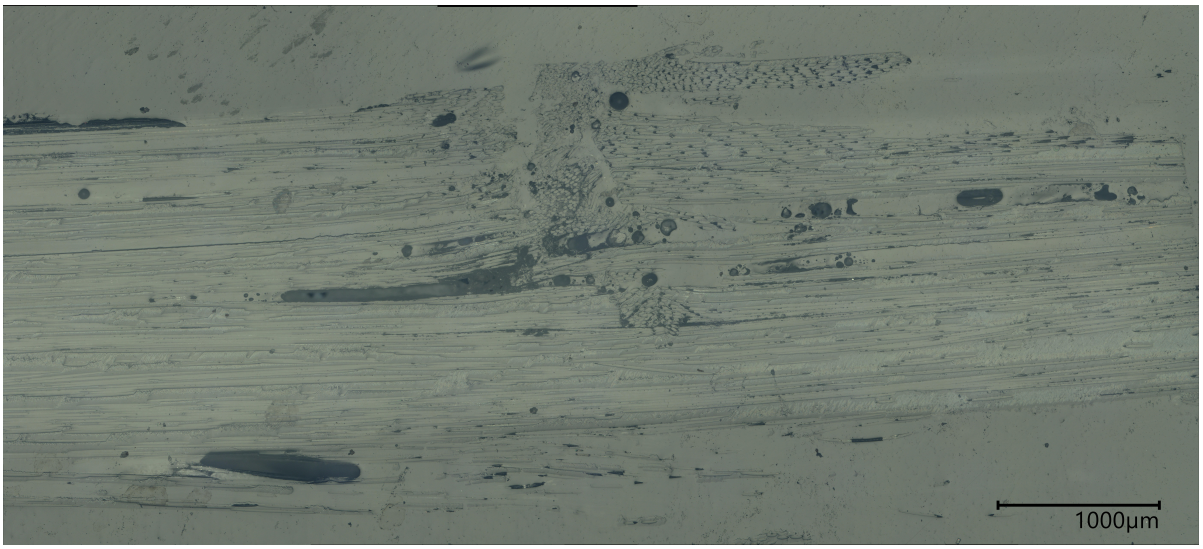

(a) Overview

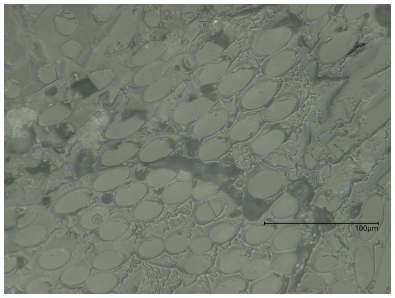

(b) Matrix Cracking

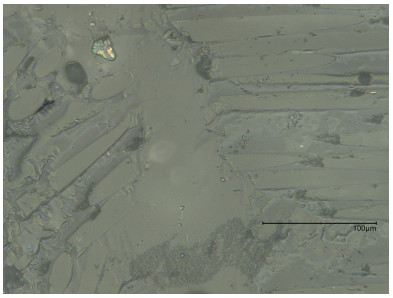

(c) Fiber Fracture

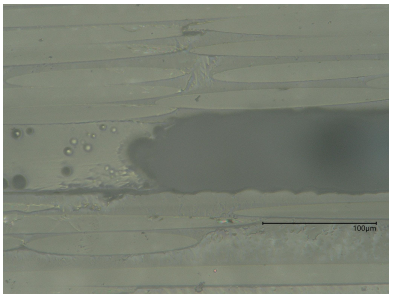

(d) Delamination

Figure 3.4: Example Micrograph of 0° specimen [x300] with details [x1000]

Chapter 4

Theoretical Background and Expectations

Impact related research into composite materials has been done for many years. This was largely influenced by their appearance in aerospace engineering. From here, the materials found use in aircrafts and high performance land vehicles such as sports cars. The unique combination of a low density and high specific strength and stiffness makes composite materials useful in these fields.

However, as with many types of materials, composites have their own flaws which limit their usage. Up to a few years ago, the production process for this type of material - both for the material itself and for products made from it - was too complicated and expensive for widespread use. A recent surge in development of production techniques has allowed for the use of composite materials for more applications in cheaper and more varying methods.

4.1 Fiber Reinforced Plastics

The standard definition of a composite material is a material which is produced from two different materials. In the case of a fiber reinforced plastic, this is a matrix (polymer) reinforced with fibers (mostly carbon or glass). *Note: the term composite material will be used to describe fiber reinforced plastics further on in the report, even though it encompasses a larger group of materials.* As can be expected, a large variety of materials can be designed that meet this requirement. From this, it can also be concluded that composite materials combine the advantages of the polymer (its low density and form ability) and the fiber material (high strength and stiffness in the longitudinal direction).

One method of describing composite materials is by looking at the length of the fibers. This method leads to two groups of composite materials: short and continuous fiber reinforced composite materials. Besides the obvious difference in fiber length, these two groups also have different production techniques. When creating products or parts from these two groups of materials, the components are either already combined (for short fibers) or will combine during the production process. In the case of the continuous fibers, the fiber bundles, mats or weaves will be impregnated with the liquid polymer. In order to ease this process, highly viscous polymers are often chosen.

In order to express the amount of fibers within the material, the so-called fiber fraction [%] is used. A fiber fraction of 0% stands for a complete polymer whereas a fiber fraction of 100% stands for just fibers as it is determined based on the volume fraction. The fiber fraction can vary throughout the material due to the design of the composite. Therefore, a material can have higher and lower local fiber fractions.

4.1.1 Material Properties

Due to their complexity, composite materials have a very specific set of material properties. These properties are dependent on both the fiber and matrix material. A relative contribution to the overall properties of the composite is shown in figure 4.1. Hereby it has to be noted that the actual influence is very much dependent on the material selection for the matrix and fibers.

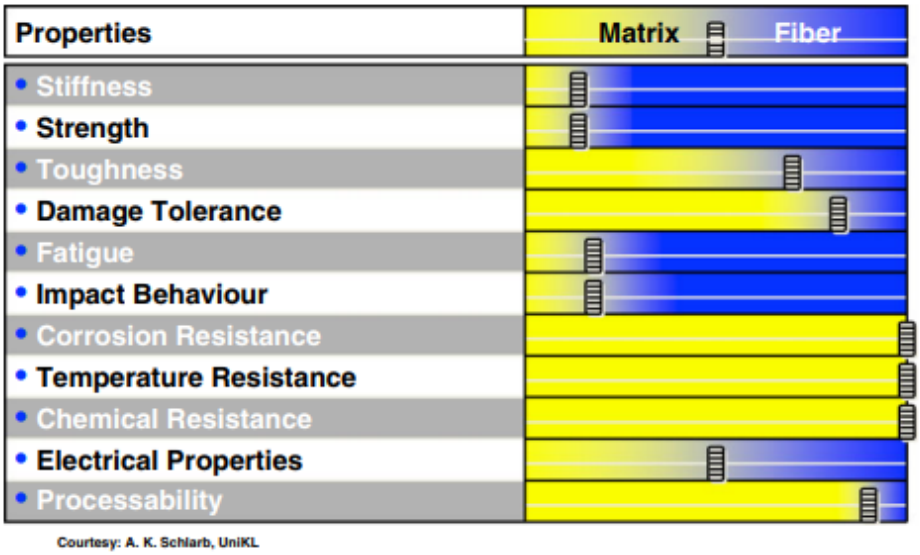

Figure 4.1: Relative influence of the matrix and fiber on the material properties, (courtesy of [28])

Asides from the influence of both elements to the properties of the entire composite material, their combination also influences the material properties. This is especially the case for the mechanical properties as the synergy between the fibers and matrix can strengthen and toughen the composite by increasing the amount of work required to fracture it [20]. The reason for this is that the matrix is mostly ductile - either plastic or elastic. During tensile or failure testing, as the broken ends of the fibers (which have already failed at that point in time) pull apart, elastic deformation or plastic flow within the matrix material exerts shear forces which gradually build back stress into these fiber ends. This type of load transfer between matrix and fiber causes the fibers to keep contributing reinforcement to the composite, even after initial failure. Furthermore, the matrix somewhat limits the stress buildup in the remaining intact fibers, causing the composite to be able to withstand larger amounts of stress before fracturing [28].

4.1.2 Matrix Material

Nearly all polymers can be used as a matrix material. Due to the large range of polymer materials available, each has their own (dis-)advantages for use in different applications. Polymers can be differentiated into two different types: thermosets and thermoplastics. The main difference between their classification is the possibility to be molten down and reshaped after the initial forming process. Thermoplastics have this capability and are therefore recyclable, whereas thermosets irreversibly harden from a soft solid or viscous liquid resin by curing.

Due to this major difference, thermosets are mostly molded directly into their final shape. Thermoplastics are mostly produced into tiny pellets which can then be melted and further processed. Thermoset polymers are mostly used in the production of composite materials.

4.1.3 Fiber Material

Most commonly, glass and carbon fibers are used in composite materials. Glass fibers are relatively weak in comparison to carbon fibers, but, due to their low cost price, are still frequently used in a large number of appliances. Carbon fibers are mostly implemented in high performance composite

materials that require large amounts of specific strength and stiffness throughout. Carbon fibers are also more expensive but in most appliances, their effectiveness is far more important.

New technologies in fiber development include that of aramid fibers (also known as Kevlar). These fibers are mostly used in military and aerospace appliances due to their excellent heat resistance and high strength.

4.1.4 Lay-Up

The fibers can be arranged in a large variety of manners. For short fibers, this arrangement is always completely random as the short fibers are mixed into the polymer melt. Since the continuous (or long) fibers are arranged during production, their directions and lay-up can be chosen. The resulting material can be called a composite laminate as it contains different layers of the two materials.

Long or continuous fibers have become the dominant form of matrix reinforcement. This is due to their more efficient reinforcement of the matrix as well as the possibility to control their orientation. Load transfer between the matrix and fiber occurs via shear forces acting on the surface between them both. Having a larger surface area therefore allows either higher shear forces (due to the smaller shear stress in the fibers) or a general lower shear stress within the material.

Ideally, the surface area must be large with respect to the corresponding cross sectional area. For most reinforcements, an ideal ratio between the length and diameter is about 100:1. This is also known as the aspect ratio of the fiber (AR). Obviously, this is dependent on the strength of the fiber, the matrix and the degree of bonding between the two [31, 27].

One possible method is to arrange the fibers in strands. This leads to a single fiber direction throughout the material, also known as a unidirectional fiber direction [0°]. The main advantage of this lay-up is the high strength and stiffness in the fiber direction. However, in the perpendicular directions to the fiber length, the material is quite weak as the properties are fully dependent on the weaker matrix material.

In order to counteract this, different weaves consisting of strands of fibers can be created. These weaves are symmetrically build up in a combination of [0/90°]. This prevents the problem of the weaker strength in perpendicular direction due to the fiber presence. An example of a multi-directional composite laminate is shown in figure 4.2. However, the fiber lay-up still contains a similar problem to that of the unidirectional strands; poor shear properties.

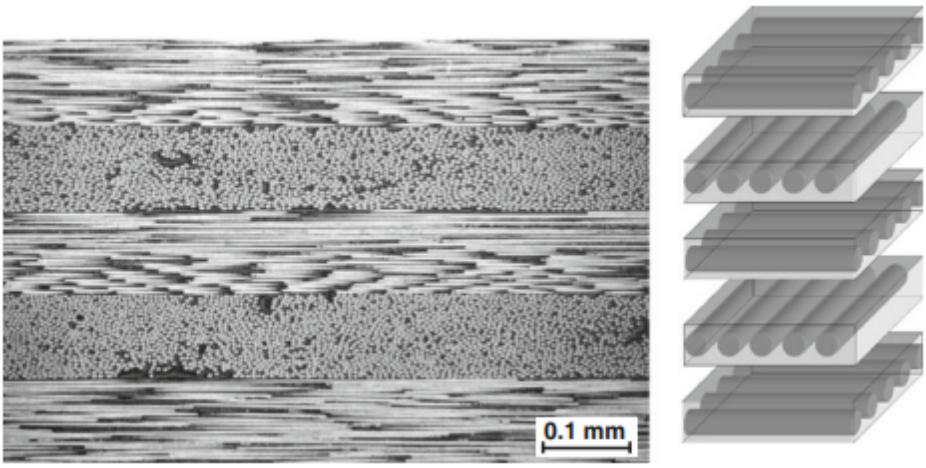

Figure 4.2: Example of a [0,90,0,90,0] composite laminate, (courtesy of [28])

In order to solve this problem, it is possible to implement strands at [45/-45°] angles. These can be a weave on their own, or in combination with the previously mentioned weave of [0/90°] strands. This

type of weave is ideal for appliances that are loaded in transverse, longitudinal and shear directions. If a part is solely loaded in shear direction, a [45/-45°] is most suitable.

It is of great importance to determine the load cases for the part to be designed before choosing/designing the composite material for said part. As mentioned above, different lay-ups are suitable for different load cases. Just adding more fiber directions to allow all types of loading cannot be done. This is due to the amount of fiber present in the composite. There can be large differences between composite materials with a fiber fraction of 40%. If the entire fiber quantity is unidirectional ([0°] for example), this will lead to the highest strength and stiffness in the fiber direction. However, adding different directions means having a smaller fiber quantity in the [0°] direction due to their placement in a [90°] direction. The strength and stiffness in the [90°] direction will drastically improve due to this design choice, but those in [0°] direction will decrease due to the smaller fiber quantity.

As with the material choices, the fiber lay-up has a large influence on the properties of the composite material. Research done on the material therefore has to contain information about the lay-up and comparative research into different lay-ups is desirable.

4.2 Failure

Due to their complex structure and properties, composite materials have similarly complex failure modes and behavior. In this, it is important to properly define a number of terms that will be used throughout this section and the entire thesis. A failure mode is a specific event through which energy is dissipated that alters the structure of the composite in such a way that it loses its original shape, form or internal structure. The failure behavior consists of the entire set of failure modes that happen during an event that causes failure, e.g. an impact event. Therefore, the failure behavior consists of a number of failure modes happening either simultaneously or sequentially. Finally, the failure criteria are the set of properties which define when and how the material fails. These include (but are not limited to) the energy absorption capability, yield stress and maximum deformation. As with the material properties, these failure criteria are heavily influenced by the choice of materials and the laminate design.

The failure modes themselves can be divided into three different categories; matrix-, fiber- and fiber-matrix interface-related failure modes.

4.2.1 Matrix Related Failure Modes

Since the matrix is the 'weakest' part of the composite, failure within the matrix itself can be quite common. However, due to its 'weakness', it is also the most ductile part, allowing large deformations before failing. A lot of energy is required for this deformation. This energy can therefore not be used as a way to create fractures/fail the material. This type of failure can be compared to 'normal' failure of the polymer material, as described by Roetling [49] for example. The most common types of matrix related failure modes are listed below.

- **Matrix Cracking**: Especially common in impact, matrix cracking is a relative simple form of failure in which a crack forms within a matrix layer of the composite material. This type of failure costs a relative small amount of energy to initiate and therefore also has a relatively small influence on the material properties [14]. This can also be seen in figure 4.1, due to the small influence of the matrix itself on the mechanical properties of the composite material. Matrix cracking occurs due to property mismatching between the fiber and matrix material, i.e. the difference in strength and stiffness/compliance between the matrix and fiber material is too large [48].

  This type of damage is based on the ultimate out-of-plane (τ^u_{xz}) and in-plane (τ^u_{xy}) shear strengths [22]. If the shear stress within the material reaches values higher than the shear strength of the material, this will causes cracks within the matrix. In the case of a [0/90/0°] composite laminate, these cracks will likely form a shape similar to that in figure 4.3. Herein, a clear type of shear

crack can be seen, which are inclined at an approximate 45° angle. These types of matrix cracks form due to high transverse shear stresses which are related to the contact force and contact area [19].

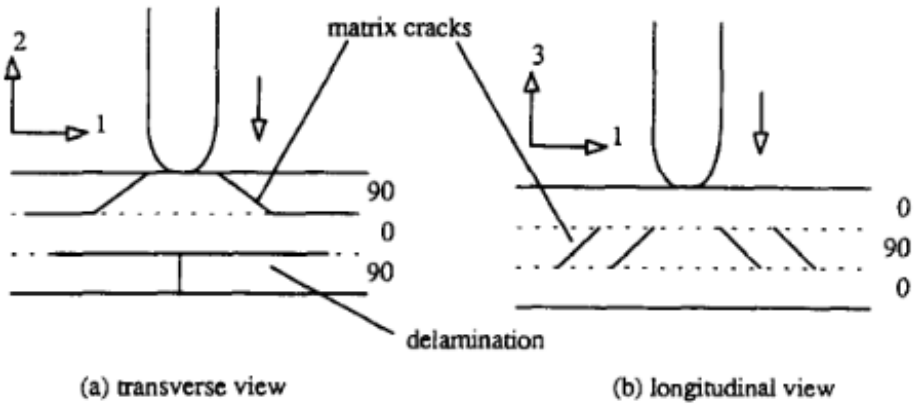

Figure 4.3: Initial damage in a [0/90/0] composite laminate (courtesy of [48])

Furthermore, a single vertical crack at the bottom of the laminate can be seen in figure 4.3. This is known as a bending crack as it forms due to the high bending stress at the bottom of the laminate. The bending stress itself is closely related to the flexural deformation of the laminate [41]. For the case of a laminate which includes a 90° (or transverse) layer, such as the one shown in figure 4.3, research by Choi et al. [18] showed that the matrix cracks in the aforementioned layer are mainly caused by the effects of σ_{11}, σ_{13} and to a lesser extent by σ_{33}, as seen in figure 4.4. Their research also concluded that there is a minimal energy limit below which no damage occurs.

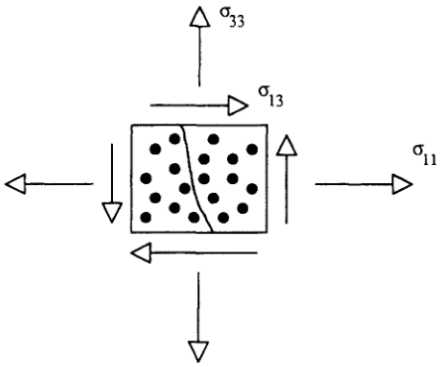

Figure 4.4: Stress components contributing to a bending matrix crack in a 90° layer (courtesy of [48])

The type of matrix cracks that occur is highly dependent on the structure of the impacted specimens, as emphasized by Cantwell and Norton [13]. Shorter and thicker specimens will form mostly cracks in the regions near the impactor as they mainly form due to high peak contact forces. Longer and thinner specimens tend to bend more during the impact, thus causing bending cracks due to the excessive flexural deformation.

This type of failure mode is also known as **intralaminar cracking**.

The bending crack is found in pure isotactic polypropylene, as described by Zebarjad et al. [66]. Herein, quasi-static three and four point bending tests were used to determine the failure behavior of pure iPP. It is important to note that their work was based on notched specimens (on the non-impacted side of the specimen) and was executed with a crosshead speed of 1 mm/min.

One of the main points found by Zebarjad et al. [66] was the non-linearity within the force-

displacement curve which is caused by the forming of craze-like failure. Before this craze-like failure occurs, the force-displacement curve shows linear behavior. Their research found that this point was reached at about 60% of the maximum bending moment. In addition to this, the formation of a stress-whitened zone was noticed. For clarification, the stress whitening definition given by ASM International [33] is presented: "Stress-whitening is a generic term for a combination of microscopic events that cause a whitened or foggy look on polymers under stress. It is thought that a primary cause for this behavior is the presence of microvoid clusters which are of a similar or greater size than the wavelength of light. These microvoids can be caused by delaminations or material failure around fillers or cavities. Although accounting for a visual change, the load bearing capacities of a material may not be substantially reduced by this effect."

Zebarjad et al. find that the stress-whitening zone begins forming before craze initiation. This is a small contradiction to similar studies on different materials (see references within [66]) which prove an inverse effect, i.e. craze forming leads to stress-whitening.

It is important to note that with an increasing load, the crazes within the pure iPP grow further and the stress-whitened zone spreads. The craze growth causes the further nucleation of new crazes to form a dense bundle. Herein, a microcrack initiates which continues to grow at increasing loads before brittle failure. A small shear yielding effect is also noticed.

This shear yielding is further evaluated by Jang et al. [35]. They state that crazing and shear yielding can both be the dominant failure mode in polypropylene. Tensile tests were conducted over a wide range of temperatures and strain rates. It was concluded that for a given test temperature, when a certain strain rate is exceeded, crazing becomes the dominant failure mode. Vice versa, for a given strain rate, a certain temperature exists above which shear yielding becomes the dominant failure mode. Concluding, higher deformation rates/lower temperatures favor crazing and lower deformation rates/higher temperatures favor shear yielding.

4.2.2 Fiber-Matrix Interface Related Failure Modes

As mentioned in the previous section, the mismatching of properties between the fiber and matrix material can cause serious failure in the composite material. This category mostly contains failure modes that are related to the disassembly of the composite laminate - also known as delamination. In other words, the composite laminate will split up into separate layers of the matrix and fiber material or a single layer will split into separate layers. The most common types are listed below.

- **Interior Delamination**: As already shown in the section about matrix cracking, in figure 4.3, interior delamination is the splitting of layers within the composite laminate. This can be caused by the further growth of an already existing matrix crack. It is also possible that an interior delamination occurs due to the misalignment between different fiber orientations of plies [1]. This will mostly occur at lower energy levels.

  Higher energy levels can lead to a larger number of delaminations and matrix cracks, along with a larger length for the cracks themselves. This can clearly be seen in figure 4.5. One of the most important factors when determining the influence this delamination has on the structural properties of the material is this length and the corresponding crack growth [15]. This is due to the stress distribution which is associated with this crack growth.

  The stress distribution within the material is dependent on its thickness and lay-up/laminate layers. Altering this by introducing a delaminated crack within or between the layers can cause higher stress levels at local level. This will lead to a larger variety in stress levels throughout the material. Interior delamination can therefore have large effects on the strength of the composite material in the long term.

  Two types of delamination can be distinguished, these are appropriately named type I and type II. Both types start of via a matrix crack and differ based on the driving force/load that

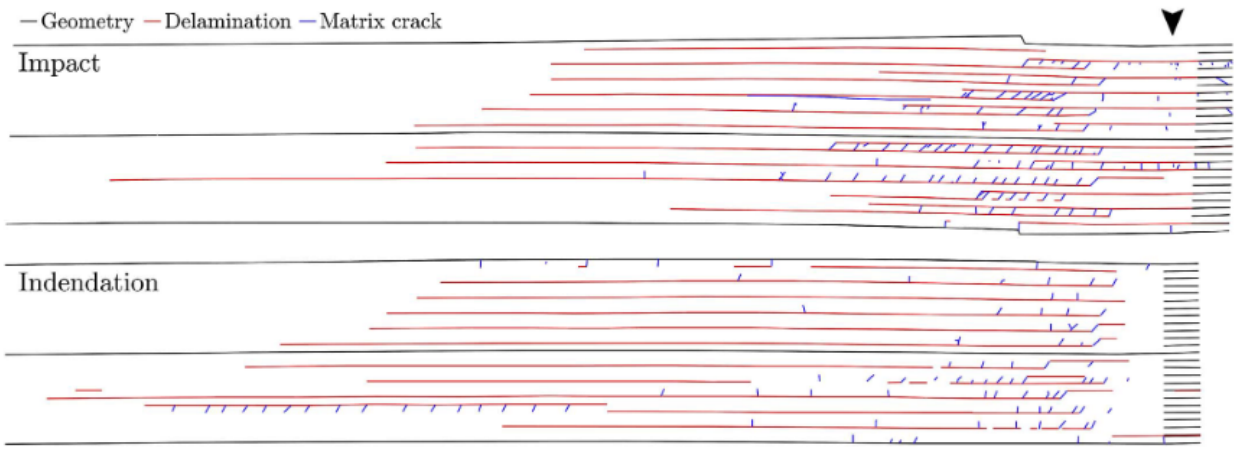

Figure 4.5: Characterized damage in a Cross-Ply Carbon/Epoxy Composite Laminate (courtesy of [53])

propagates the crack. **Type I** delamination is based on peel forces, or normal forces on the surfaces, drawing the layers apart. **Type II** delamination is based on shear stress/shear forces sliding the layers apart from eachother. When researching the specific type of delamination, a double cantilever beam setup is used for type I, whereas an end-notched flexure test is used for type II [8].

One of the main causes of delamination is the weak bonding between the fibers and matrix of a composite material. This is mostly due to a poor material selection [38].

- **Fiber Pull-Out**: Weak bonding can also lead to another failure mode known as fiber pull-out. In this case, the longitudinal force on the fiber is stronger than the bonding between the fiber and the matrix, thus 'pulling' the fiber out of the matrix. In other words, the bonding between the fiber and matrix cannot cause enough friction to counteract the pulling force on the fiber.

  If this occurs, the fiber in itself will remain intact and there will be a fiber shaped hole in the matrix. This has a double negative effect on the structural properties of the composite. Firstly, the reinforcing element (the fiber) has been removed, which leads to a local decrease in fiber volume fraction. This diminishes the structural properties of the material. Secondly, a hole remains within the matrix. Holes themselves provide no structural rigidity at all to the material, thus causing even further devaluation of the material properties.

  Due to the complexity of this failure mode, it is relatively uncommon in impact properties as this usually involves forces and stresses in directions other than the 'pulling' direction of the fibers. Especially in continuous fiber reinforced plastics, a complete fiber pull out is rare due to the length of the fibers themselves. For short fiber reinforced plastics, the pull-out of a single fiber has little influence on the material properties due to the small changes in fiber fraction.

  In short, it is possible that high shear and pulling forces together can pull a fiber away from its location, resulting in an air pocket within the matrix. This is a severe weak spot and can cause further failure of the material. However, it is unlikely that a complete fiber pull-out is achieved before other failure modes are engaged, such as fiber/matrix debonding.

- **Fiber/Matrix Debonding**: As the name may already suggest, fiber matrix debonding is the splitting of fibers and matrix material within the composite. The growth of these debonds is one of the main mechanisms of damage evolution, especially for unidirectional composites [46]. A fiber matrix debond usually occurs after a fiber breakage (as will be discussed further below). This is due to the amount of energy being released during the breaking of a fiber which is larger than the energy required for the fiber to break. The extra energy then is absorbed by the material via a debonding of the fiber and the matrix.

As can be expected, this will cause a chain reaction. The first fiber break and accompanying fiber matrix debonding will lead to a decrease in structural properties of the composite material surrounding it. Therefore, it is more likely to also fail in its vicinity via means of another fiber breakage or growth of the fiber matrix debond that is already present. Varna and Pupurs [46] have created a Finite Element Model of the energy release that accompanies a fiber breakage within a unidirectional thermoset composite material. From this, it can be determined if and to what extent a fiber matrix debonding process will occur.

To summarize, there are 3 main categories of fiber/matrix bonding related failure modes. Two of them are caused by the weak bond between the fibers and matrix material (and a failure within the matrix), whereas the other is the result of a previous failure within the fibers. Although the failure modes may sound similar, there are some key differences in the resulting failure pattern.

After delamination, a clear split in layers can be observed. For reference, it can be thought of as a book. When intact, the book is closed, thus giving a solid layer whose thickness is the sum of that of all individual layers. After delamination failure, the book is opened at either one or multiple locations, allowing visible splits between layers (or pages). Delamination failure therefore can be classified as 'clean' failure due to its layer based behaviour.

Fiber matrix debonding is similar to delamination, with the difference being the cleanliness of the debonding. The crack which represents the debonding is not in a straight line (as with delamination), but will follow the fibers within the material. Therefore, the crack is rough. Furthermore, fiber matrix debonding will cause the matrix material to partly tear away from the fiber, thus leaving the fibers partly exposed after failure.

Fiber pull-out can also be classified as a 'clean' failure mode if the fibers are pulled out far enough. The fiber pull-out will leave the fiber displaced and the matrix material with a fiber-shaped hole. Obviously, the hole is not perfectly fiber shaped as it is highly unlikely that in the case of an impact or non-experimental situation, the force is exactly aligned with the fiber, thus allowing it to drag along the matrix and creating a rough and non-fiber-shaped hole. Remains of the matrix on the fiber are commonly found and prove a stronger bond between the fiber and matrix when compared to a fiber being pulled out cleanly.

4.2.3 Fiber Related Failure Modes

Fiber related failure modes happen at high impact energy events, given that the fibers are the strongest part of the composite laminate. Failure within the fibers requires a lot of energy, which also makes it a failure mode that absorbs a large amount of energy. The latter part is useful when designing materials which have to absorb a lot of energy. However, after fiber failure, the structural properties of the composite material decrease significantly due to the influence of the fibers. As with the matrix cracking failure mode that was previously discussed, there is a single fiber related failure mode that speaks for itself:

- **Fiber Breakage**: This type of failure occurs due to high stress fields and indentation effects. The impacting object induces a shear force and high bending stresses on the other side of the specimen [50]. These high bending stresses will overload the fibers, thus breaking them. As mentioned before, the fibers usually have excellent structural properties (in at least 1 direction). Reaching bending stress levels capable of failing the fibers therefore requires a lot of energy. Besides the high energy levels, there are some other contributing factors to the fiber breakage, as discussed by Talreja [57]:

  Firstly, as mentioned, the fibers have excellent properties in their main direction. Therefore, a load/stress that is applied parallel to the fibers can cause them to fail earlier, as their respective properties in those directions are smaller.

  Secondly, there can always be small failures or weaknesses within the individual fibers. These local weak spots can handle less stress than the rest of the fiber, thus causing failure of the

entire fiber. If a single fiber fails, this leads to an increase in load that has to be handled by the other fibers (in relative terms, as the total load doesn't change). With the remaining intact fibers having to handle a larger load/stress, it is possible that they fail as well. This can cause a chain reaction which eventually can end in the total failure of the composite material. This is shown in figure 4.6.

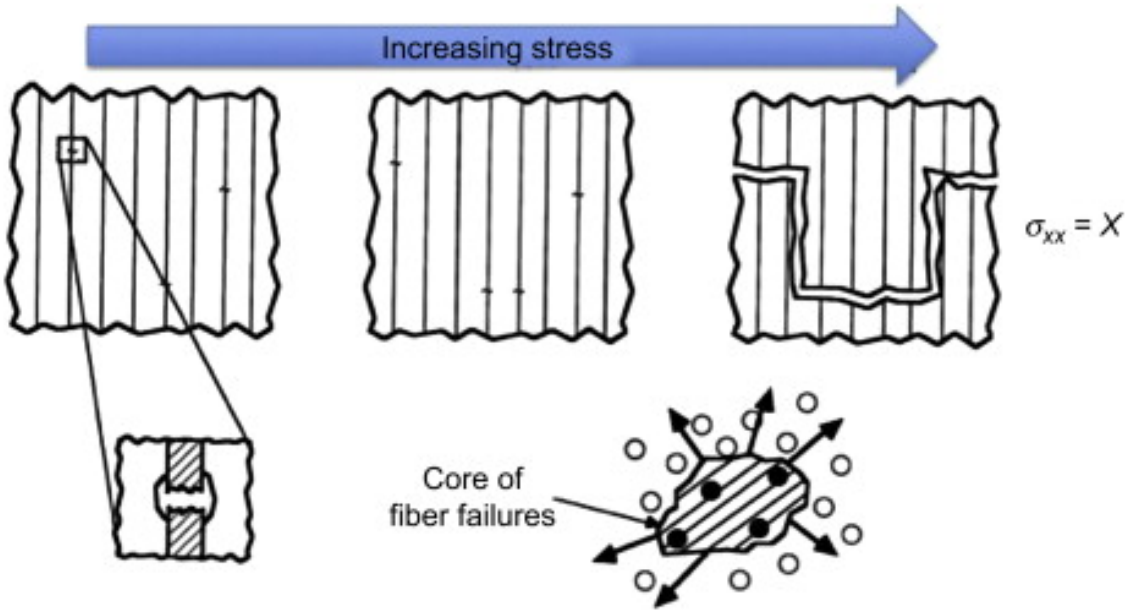

Figure 4.6: Schematic illustration of the sequence of failure events leading to failure under imposed axial tensile loading (courtesy of [57])

The chain reaction mentioned is causes by the failing of several fibers, which causes local weak regions within the material. Matrix cracks can then form between these failures, thus causing a core of failures (as seen in figure 4.6), which in itself produces a crack-like entity that grows throughout the material until it completely fails.

4.3 Rate-dependency

One of the unique aspects of plastics and composite materials is their material properties. The complex relation between matrix and fiber material yields a combination of their respective properties. A further addition to this already complex system of properties is that of rate-dependency. When talking about the 'rate', the strain rate is meant. The strain rate itself is defined as the change in strain (deformation) of a material with respect to time [44].

Two major types of events can be distinguished: low and high strain rate events. The latter are events which happen in short periods of time, thus favoring the elastic properties of the material. As expected, low strain rate events have a much longer duration, either due to the type of testing/event occurring or due to the materials high impact resistance or toughness.

The rate dependency of polymers has been a research topic for a long period of time. Walley and Field investigated the properties of 17 different polymers over a rate range of $10^{-2} - 3 \text{ x } 10^{4}\ s^{-1}$ [63], in which they also stated the effects of deformation rate at molecular level. It was found that there was a range of different behaviours within the polymers, based on their molecular structure, thus strengthening the importance of material selection. This was also confirmed in a review done by Jordan and Siviour [52] in which the differences between types of polymers and research method were investigated.

The rate dependency of fibers is a more complex mechanism. It is known that fibers can be made

from a large variety of materials, thus resulting in a large difference in behaviour. Harding and Welsh [29] found that glass fibers showed rate dependent material behaviour, whereas carbon fibers did not. This was proven by executing a series of tensile tests at different strain rates and determining the material properties based on the corresponding results.

Arao et al. [3] did extensive testing and modeling on the rate dependency of glass fibers. They state a number of arguments for the rate dependent strength behaviour - which should increase at higher strain rates - of glass fibers. These possible causes for the strain-rate dependence for the strength of glass fiber are: (1) a temperature rise during the test, (2) modification of the molecular structure, (3) the effect of thermal residual stress in glass fibers, (4) the effect of a stress wave, and (5) the propagation of surface flaws during the test. Because the strain-rate dependence in carbon fibers is extremely small, the strain-rate dependence in glass fibers may be caused by the unique characteristic of glass.

4.3.1 Stiffness

One of the material properties that is influenced by the strain rates is the engineering stiffness (E_i), also known as the direction dependent stiffness ($E_i(\dot{\epsilon}_i)$) [30]. In figure 4.7, the in-plane engineering stiffness in different directions is shown for a multi-layered weft knitted fabric (MKF) consisting of Polypropylene (PP). It shows that an increase in strain rate leads to an increase in stiffness.

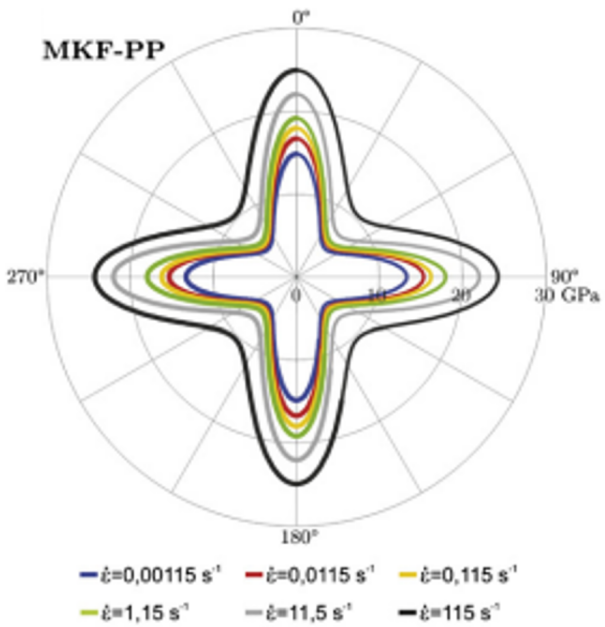

Figure 4.7: Polar plot of in-plane engineering stiffness for different strain rates (courtesy of [30])

When inspecting the figure, it becomes clear that the increase in stiffness is not easily definable. This is due to its dependence on the natural logarithm of the strain rate divided by a reference rate, as defined in equation 4.1 [30] which is based on work done by Johnson and Cook [36]. In this equation (and further on) A_i^E denotes a material constant and $E_i^{(ref)}$ the reference stiffness at reference strain $\dot{\epsilon}_i^{(ref)}$. These material constants can be determined via testing by choosing the reference points.

$$E_i(\dot{\epsilon}_i) = E_i^{(ref)} \left(1 + A_i^E ln \frac{\dot{\epsilon}_i}{\dot{\epsilon}_i^{(ref)}}\right) \quad (i = 1, 2) \tag{4.1}$$

4.3.2 Tension and Compression

Similar to the elastic properties (i.e. the engineering stiffness of the previous paragraph), the strain rate dependent tension and compression strengths $R_i^{+/-}$ can be formulated. This is done in equation 4.2, in which a material constant A_i^R and a reference strength $R_i^{+/-(ref)}$ are used. Similarly, these constants can be determined via testing by selecting the reference points.

$$R_i^{+/-} = R_i^{+/-(ref)} \left(1 + A_i^R ln \frac{\dot{\epsilon}_i}{\dot{\epsilon}_i^{(ref)}} \right) \quad (i = 1, 2) \tag{4.2}$$

4.3.3 Failure Modes

Given the dependence of the material properties on its failure, it can be expected that the failure modes themselves are also heavily influenced by the strain rate. A lot of research finds a relation between the amount of failure (i.e. the affected damaged area) and the strain rate. An example of this is the work done by Kim et al. [39] which focuses on difference in affected damage area at different levels of impact energy. They found that a certain energy level was required to cause both internal and external damage to the specimen (similar to Aktas et al. [1]). Furthermore, at certain energy levels, fiber damage was introduced, as well as delaminations at even higher levels of impact energy.

Cui et al. [21] looked into the different failure modes at different strain rates for a long glass fiber reinforced polypropylene, similar to this thesis. Their research focused on the tensile properties and failure. Their work showed an increased brittleness at higher strain rates. Under low strain rate, they found that fibers that were pulled out of the matrix were relatively smooth, those pulled out due to higher strain rate had more PP resin attached to them. This would lead to the assumption that the matrix fiber bond becomes stronger at higher strain rates.

Fiber debonding and interfacial pull out were the main failure modes (for 0° specimens) at low strain rates. Fiber fractures were also found. These increased in number with an increase in strain rate. On the contrary, the fiber pull-out decreased at higher strain rates. It appears as if the fiber fracture failure mode took over the energy absorption from the fiber pull-out. Finally, they found an increased amount of ductile fibril pulling at higher strain rates. The main failure mode was still brittle, but these fibrils indicate a higher fracture toughness at higher strain rates.

Okereke et al. [45] also investigated the strain rate influence on failure modes of glass reinforced polypropylene. Their research was focused on the compression failure behavior. It was found that at low (between 10^{-4} and $10^{-1}s^{-1}$ and medium ($10^{1}s^{-1}$) strain rates similar failure occurred in 90° specimens. This failure was interlaminar matrix failure/cracking along a clearly defined fracture plane within the material, at the point of impact. The failure seemed equal for medium and low strain rates, although due to an error in the set-up, the moment of failure for the medium strain rate tests was not captured. Tests at even higher strain rates (up to $10^{3}s^{-1}$) led to more brittle failure on multiple crack fronts.

4.4 Impact Energy

When researching the effect of impact on a material, it is of great importance to understand and define the type of impact and to quantify it. The main factor for quantifying the impact is by looking at the energy level. Impact in itself can be seen as contact between at least two bodies, each with their own given velocity and geometrical properties, with a short duration of time. The time factor is of importance as to rule out the influence of long term effects (such as fatigue).

Given the definition of impact, determining impact energy can be done by looking at the energy levels of the bodies themselves. At the moment of impact, it can be assumed that the only energy present is kinetic energy in all bodies. In a car crash for instance, the value of the kinetic energy is much larger

than that of for instance the potential energy, thus allowing only the kinetic energy to be taken into account.

The standard notation for the kinetic energy of a single body i is:

$$E_{k,i} = \frac{1}{2} m_i v_i^2$$

4.4.1 Dual Body Impact

In the case of a multibody impact, the total impact energy is a sum of the impact energies of the individual bodies. However, hereby it is of great importance to define the direction of the vector v in which the impact energy should be calculated. It can easily be imagined that the impact energy of a collision is heavily dependent on the angle of the impact, as well as the difference in velocity between the bodies. A head-tail collision between two vehicles can only exist if there is a difference in velocity in the first place.

For example, the impact energy of a head-tail collision between two vehicles; A travelling at $v_A = 60km/h$ and vehicle B travelling at $v_B = 50km/h$, can be calculated by taking the difference in kinetic energy of both vehicles as the velocity is in the same direction. The mass of vehicle A (m_A) is set to be 20% more than that of vehicle B, thus $m_A = 1.2m_B$. The total calculation is shown below:

$$E_{I,head-tail} = \frac{1}{2} m_A v_A^2 - \frac{1}{2} m_B v_B^2 = 166.73 m_B - 96.47 m_B = 70.26 m_B J$$

Using the same vehicles A and B, now travelling directly towards each other and thus causing a frontal collision, a major difference in impact energy can be noticed. In this case, the total energy is the sum of both kinetic energies. This leads to an impact energy as shown below:

$$E_{I,frontal} = \frac{1}{2} m_A v_A^2 + \frac{1}{2} m_B v_B^2 = 166.73 m_B + 96.47 m_B = 263.20 m_B J$$

The final clear case of determining the impact energy in a two body situation, simplified to a car crash situation, is the T-Bone impact. This occurs when one of the vehicles impacts the other one in the side at a perfect 90 ° angle. In this case it can be assumed that only the kinetic energy of the vehicle which comes in from the side is of importance. As can be seen from the first equation, this value is either $166.73 m_B$ or $96.47 m_B$ J, dependent on which of the vehicles is chosen.

It can be concluded that the maximal impact energy in a two body impact situation is achieved when the velocities of the bodies are in exact opposite direction (sum of the kinetic energies). Similarly, the minimal impact energy is achieved if both velocities are in equal direction. All other impact events between two bodies have impact energies ranging between these extreme values. It has to be noted that the total impact energy has to be positive if there is any form of impact!

Maximal impact energy for an impact situation with two bodies (A and B):

$$E_{I,max} = \frac{1}{2} m_A v_A^2 + \frac{1}{2} m_B v_B^2$$

Minimal impact energy for an impact situation with two bodies (A and B):

$$E_{I,min} = \frac{1}{2} m_A v_A^2 - \frac{1}{2} m_B v_B^2$$

To conclude, it is desirable to have a formulation for the total impact energy in an impact situation which contains two bodies with individual masses, travelling at individual velocities. To clarify, the bodies are once again denoted by A and B. It is important to note that body B is traveling in the 0°

direction, such that v_B is also directed in the 0° direction. The angle between the bodies (θ_A) is 0° if the velocities are aligned, and 180° when opposite. This is shown in figure 4.8. The final equation for the impact energy as shown in equation 4.3:

$$E_I = E_{k,A} - cos(\theta_A)E_{k,B} = \frac{1}{2}m_A v_A^2 - cos(\theta_A)(\frac{1}{2}m_B v_B^2) \tag{4.3}$$

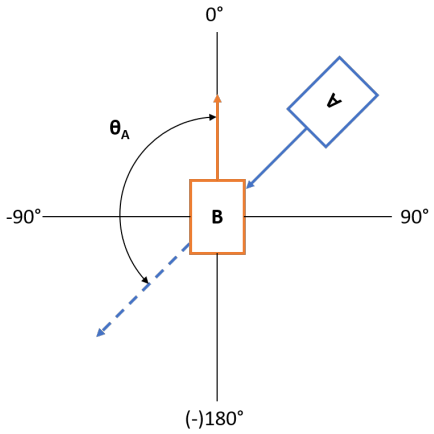

Figure 4.8: Visualization of the Impact Angle θ_A for a Two-Body Impact Situation

4.4.2 Single Body Impact

The title to this section can be misleading as there is no such thing as a a single body impact. The definition of impact in itself is, as mentioned before, the short contact between at least two bodies moving at their own individual velocities. A single body impact is equal to a dual body impact in which one of the bodies has no kinetic energy, due to the absence of its velocity. This can be compared to the 90° impact angle discussed in the previous section. In this, only the kinetic energy of one of the bodies is responsible for the entire impact energy. Therefore, the impact energy of a single body impact can be described by equation 4.4, in which A represents the body.

$$E_{I,SB} = \frac{1}{2}m_A v_A^2 \tag{4.4}$$

4.5 Energy Absorption

During an impact situation, there is always some form of energy transfer between bodies. Given the formulations for the impact energy as mentioned in the previous section, this can come in three notable forms: velocity transfer, mass transfer or energy absorption. Usually, an impact situation will lead to a combination of all mentioned forms of energy transfer.

It has to be noted that the energy transfer is never without any loss of the initial kinetic energy. This is mostly due to some of this energy being turned into heat. Friction also plays a notable role within the initial and residual energy levels, but this will be discussed in more detail further on as its influence during the impact moment itself is negligible due to the short duration of the impact event. The transfer of energy to heat and sound is outside of the scope of this thesis.

Given the type of impact situations that are being investigated in this thesis, it can be assumed that there will not be any transfer of mass/material. This is due to the low impact energies with respect to the material properties of the used materials and tests. Mass transfer will usually only happen on particle level (microscopic scale impact events) or during impact events involving huge amounts of masses (for instance in impact events between celestial bodies).

Secondly, the velocity transfer is something to keep in mind as this will definitely play a role during impact testing of the composite materials. This will be a factor if the specimen of the composite material is not clamped or fixed, which will guarantee it to always have a velocity of 0 m/s. If this cannot be guaranteed, any type of velocity gained by the specimen will lead to an amount of impact energy being converted into kinetic energy of the sample. When looking at the energy balance, this has to be taken into account, albeit with the notion that this kinetic energy will be low in comparison to the total energy level.

The most important part of the energy transfer during an impact situation is the energy absorption that happens within a composite material. In general cases, the energy absorption within a material is achieved through means of deformation and possible consecutive failure. It can be imagined that for the deformation of a material, an energy input is required, similar to a force multiplied by a distance to which is it applied. Therefore, the amount of energy required to deform the material can be determined by taking the area under the force-displacement (or: load-displacement) curve acquired from testing [44].

The energy absorption occurs due to failure and deformation of the material. It is desirable to control this energy absorption when designing a composite material. This is due to the loss of structural strength and stiffness during energy absorption (failure). As can be expected, this failure and absorption behaviour needs to be reliable to accurately predict the material behaviour. A linear decrease in structural properties is ideal as this is the easiest to predict using models.

This 'linear' behaviour can be difficult to achieve as specific failure modes have their own respective influences on the decrease in structural properties, i.e. larger amounts of energy are absorbed via these types of failure modes, but their influence on the structural properties is also large. As also mentioned during the section about delamination, the crack length has a significant influence on the structural properties of the composite material. Predicting the number of cracks and their respective length and growth rate is therefore required to accurately predict the energy absorbing capabilities of the delamination failure mode. This serves as a good example for the difficulties regarding the achievement of this behaviour by altering the design of the material.

4.5.1 Specific and Volumetric Energy Absorption

Although there are standards for the dimensions of specimens used in tests which are used to determine the energy absorption of a material, it is desirable to distinguish a property which is independent of these parameters. Therefore, two definitions of the energy absorption are used; Volumetric Energy Absorption (VEA) and Specific Energy Absorption (SEA).

The VEA, or Volumetric Energy Absorption capability, is especially useful in situations where the design has dimensional limits [44]. Hereby it is thought of energy absorbing systems which have to be fitted in an already determined location within the design. Since more volume is equal to a larger energy absorption capability (if the material remains unaltered), it is important to know what the volumetric and dimensional limits of the design are. The volumetric energy absorption capability is material dependent and relatively straightforward to use.

When there are no dimensional limits, but for instance mass limitations are present, it is desirable to use a material that has a high energy absorption per unit mass. For this, the Specific Energy Absorption (SEA) property is used. It can be calculated by dividing the total energy absorption by the mass of the specimen.

4.5.2 Energy Profiling Method

To fully define the aforementioned processes of energy absorption and transfer, a relation between the impact and absorbed energy can be determined. This is done by Aktas et al. [1] by introducing the Energy Profiling Method (EPM). In this method, the relation between the impact and absorbed energy is plotted in a graph, as seen in figure 4.9. The equal energy line in the figure represents an equal amount of impact and absorbed energy.

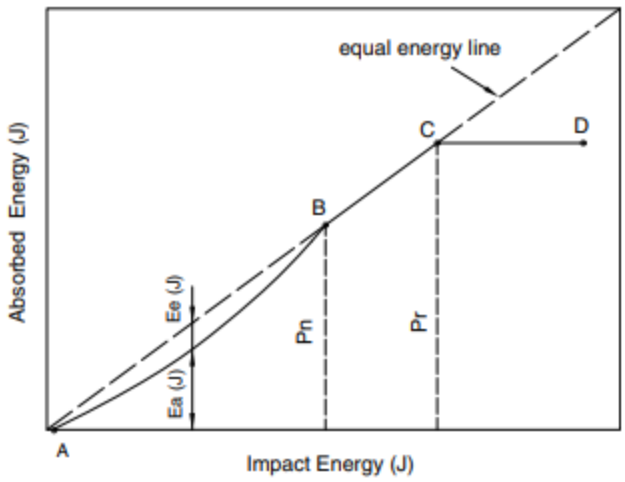

Figure 4.9: Typical energy profile diagram of a composite plate (courtesy of [1])

Three different zones can be distinguished from the figure: A-B, B-C and C-D. Each zone represents a different interaction between the impactor and the impacted specimen with a corresponding energy relation. The three zones - based on their respective ascending energy level - are: **rebounding**, **penetration** and **perforation**. Each of the zones will be explained in more detail below.

- **Rebounding (A-B)**: As can be seen in the graph in figure 4.9, the rebounding phase implies the presence of a larger amount of impact energy than that can be absorbed by the material. This residual impact energy is then transferred back to the impactor, thus giving it a velocity and bouncing it away from the material. The resulting energy equation can be written as (according to the figure):

  $$E_{Impact} = E_{Absorbed} + E_{k,Impactor} (= Ea + Ee)$$

  The rebounding phase can lead to failure within the material as there is a form of energy absorption. Due to the low energy levels, this will be of little significance. Furthermore, due to the definition of the other zones, there will only be internal damage or deformation.

- **Penetration (B-C)**: This phase is the most straight-forward due to the relation between the impact and absorbed energy. During the penetration phase, these are exactly equal. The material is therefore capable of absorbing all kinetic energy that the impactor carries by bringing it to a full stop. This principle also yields the name penetration as the impactor penetrates the material before coming to a stop once inside.

  This phase starts at the penetration threshold Pn. This is due to the fact that a specific amount of energy is required before the material is penetrated. This threshold is therefore fully dependent on the material selection and the dimensions of the specimens.

  The energy equation for the penetration zone can be written as:

  $$E_{Impact} = E_{Absorbed}$$

  An impact event which occurs in this phase will cause severe damage to the material. Due to the penetration, a lot of visible damage is present, along with major internal failure.

- **Perforation (C-D)**: Similar to the rebounding zone, during perforation, the amount of impact energy is larger than the amount of absorbed energy. However, the difference is that in the perforation zone, the maximal energy absorption capability of the material is overshot by the impact energy. This is denoted by the perforation threshold Pr. This threshold is based on the

amount of energy required for the impactor to penetrate in to the material and then breaking out on the bottom side of the specimen.

The perforation phase therefore can be seen as a straight line in figure 4.9 as the absorbed energy level will no longer increase due to it already surpassing the maximal capability. In theory, the impact energy can infinitely increase without any further energy being absorbed by the material.

The energy equation for the perforation phase can be written as:

$$E_{Impact} = E_{Absorbed} + E_{Residual}$$

Any impact event within the perforation phase leads to complete destruction of the material. The complete thickness of the material will come into direct contact with the impactor, thus destroying any matrix or fiber material present.

The energy profiling method can be very useful for visualizing impact events and grouping them. It can also be used to determine the energy absorption capabilities of the material by looking at the different phases and the thresholds. Accurately determining the thresholds is a difficult task with a high reward for further research into the material properties.

When accurately determined, material behavior and failure can be predicted when combining the energy profile with literature regarding failure at levels of energy absorption as well as experimental results. Boria et al. [12] found that impacts with higher velocities and lower masses tended to end up in the penetration phase, whereas impacts with lower velocities and higher masses tended to end up in the rebounding phase. Furthermore, they conclude that an increase in impactor mass leads to an increase in absorbed energy and stiffness, whereas an increase in velocity led to a decrease.

Chapter 5

Results

5.1 Quasi-Static Testing

5.1.1 90° Specimens

Due to the direction of the fibers, being parallel to the loading strip, it is expected that the 90° specimens have little resistance to the bending force being applied by the test. This is mainly due to the fact that the fibers are essentially ruled out of carrying the load, thus making the matrix itself the main load bearing part of the composite. The expected flexural modulus and force/displacement at failure is therefore equal to that of standard, not reinforced, isotactic polypropylene.

Given that the polypropylene itself is the load bearing part of the composite, it is expected that matrix related failure modes such as matrix cracks and fiber matrix debonding will dominate the failure behavior. As learned from the theoretical background, matrix failure usually implies a crack that will propagate throughout the material. This crack will most likely start from the bottom (the side that lies upon the supporting points) and propagate upwards until failure. This is due to the tensile stress being applied to that side of the specimen. Due to the test set-up, a complete failure (i.e. complete rupture of the specimen) is highly unlikely as the load will be released after a force drop which will occur after the first crack formation and propagation throughout a part of the specimen thickness.

Three crosshead velocities - 2, 20 and 200 mm/min - were used during testing. The used specimens and their dimensions are shown in table A.1 in appendix A.1. Figure 5.1 shows the force displacement curves found by the quasi-static three point bending testing. It will be used as a reference for explanation of some phenomena.

In the figure, a couple of relations can be noticed, starting with the most obvious: the increase in force at failure at higher strain rates. This is also shown by the flexural strength in table 5.1. This behavior was also found in tensile testing done on this material by Erartsin et al. [24] and Cui et al. [21]. There are a number of possible explanations for this behavior, including the viscous behavior of the matrix at higher strain rates and interface properties between the fibers and matrix. The behavior is also in line with Eyring's theory about viscoelastic behavior of polymers [61].

Table 5.1: Properties of 90° specimens at different strain rates

Velocity [mm/min]	Strain Rate [s^{-1}]	Flexural Strain	Flexural Strength [MPa]	SEA [kJ/kg]
2	2.03e-4	0.0072	53.1091	0.0094
20	0.0017	0.0078	58.3932	0.0112
200	0.0068	0.0084	66.6268	0.0173

From figure 5.1 it can also be concluded that the displacement at failure increases with an increase in strain rate. This is also shown as the strain (specimen dimension independent displacement) in table

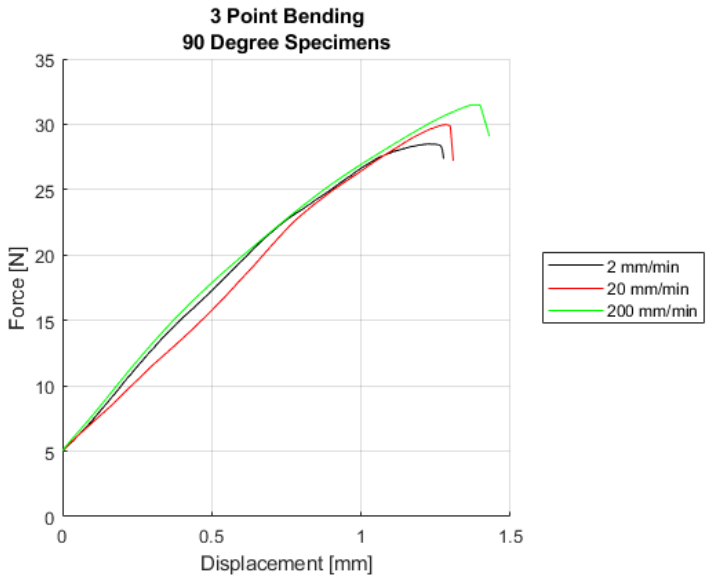

Figure 5.1: Force Displacement Curve of the 3 Point Bending Tests for 90° specimens at room temperature

5.1. This behavior once again aligns with the tensile data found by Cui et al. [21] and can also be related to the viscous behavior of the material at higher strain rates. However, this is not as originally expected, as the general assumption is that the material becomes more brittle at higher strain rates. That would mean that the deformation at failure should decrease. A general increase in brittleness was found by Cui et al., but due to local ductile fibrils and microfibrils, the deformation at failure increases.

The expectation was an increase in modulus with an increase in strain rate. The averages shown in figure 5.2a show a different story. These results would imply a drop in modulus near the 20 mm/min mark, which would be contradictory to the expectations. However, when taking the deviations into account, this cannot be concluded. Firstly, the possibility of the modulus remaining constant throughout the entire range of strain rates tested is possible. This is due to the overlap that exists throughout all deviations.

Furthermore, it is possible that the expected increase in modulus is present, once again due to the presence of the large overlap between all deviations. Since the average was taken, and the deviation for the 20 mm/min case is far lower than that of the other strain rates, it is possible that some specimens may have a large influence on this average and thus causing a skewed look at the real results. Therefore, there is no clear relation between the stiffness and strain rate. Tensile testing of the used material also proved no direct relation between the modulus and the applied strain rate.

The resulting material properties are also visually shown in figure 5.2. Herein, the white bars represent the material properties of the specimens tested at 2 mm/min, red bars represent those tested at 20 mm/min and green at 200 mm/min. These can be used to more easily identify trends within the material behavior with respect to the strain rate.

The micrographs of the specimens, as shown in figure 5.3, show similar behavior. A single matrix crack was visible in all tested specimens. An increase in strain rate led to an increase in crack depth (length of the crack in the thickness direction). The specimens failed on the non-impacted side of the specimen - the side under flexion - before the crack propagated upwards to the impacted side. This is due to the high flexural stress and strain on the non-impacted side. The matrix cracks were guided by the present fibers, creating a clear 'path' through them. All cracks ended at a dense layer of fibers that is within the material. The propagation of a crack in a fiber dense region requires more energy than that in a matrix dense region.

To conclude, no clear relation between the flexural modulus and strain rate can be found for 90°

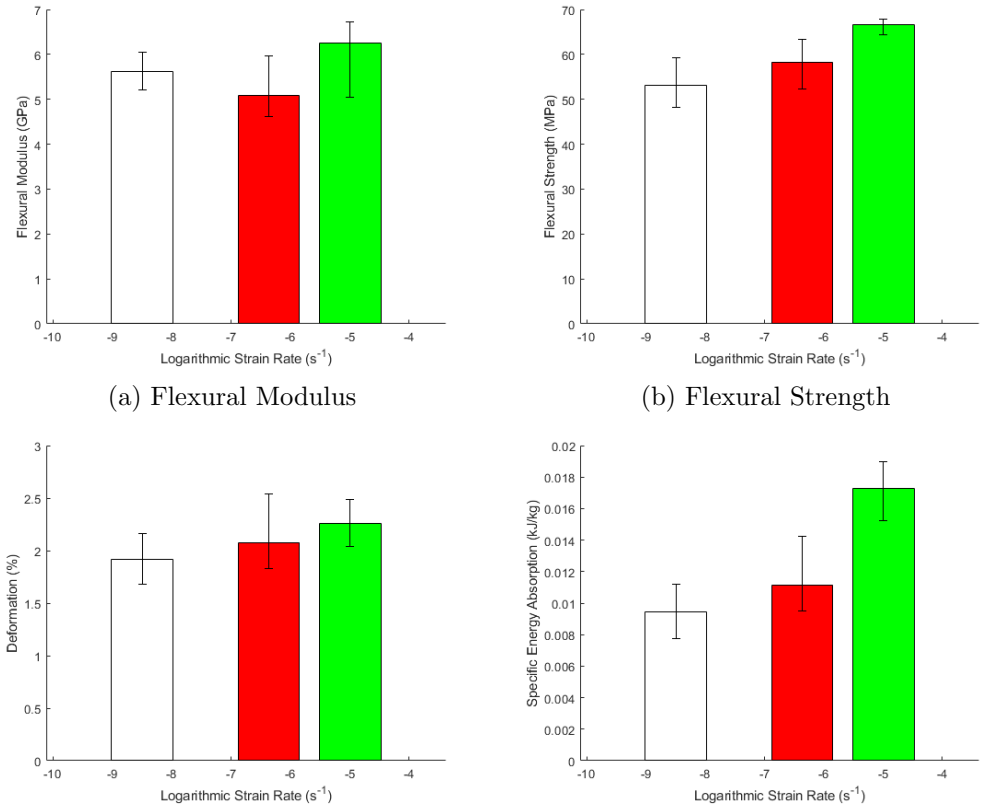

(a) Flexural Modulus

(b) Flexural Strength

(c) Deformation at failure

(d) Specific Energy Absorption

Figure 5.2: Mechanical Properties of 90° specimens at different strain rates

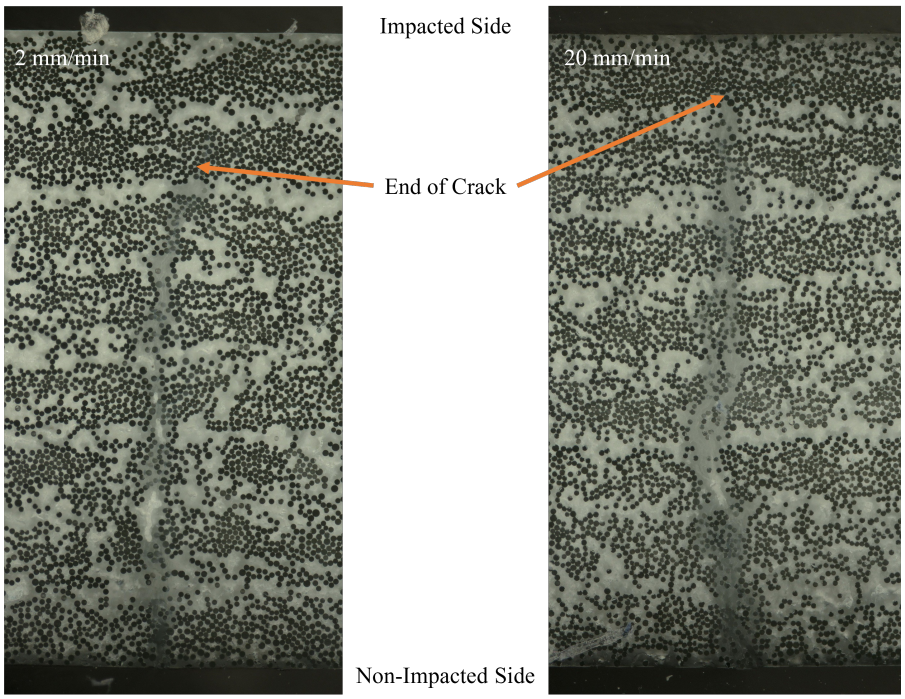

Figure 5.3: Micrographs [x300] of 90° specimens illustrating relation between strain rate and crack length; 2 mm/min absorbed 0.0094 kJ/kg, 20 mm/min absorbed 0.0112 kJ/kg

specimens. At higher strain rates, there is an increase in flexural strength and strain at failure, which is in line with data found in tensile testing. A single matrix crack propagating from the non-impacted side of the specimen was found in all specimens, but its propagation was highly rate-dependent. Higher

strain rate means a deeper crack throughout the material and a higher energy absorption.

5.1.2 0° Specimens

The 0° specimens are loaded in a direction perpendicular to the fiber direction. The main load bearing capacity of the composite is therefore transferred to the fibers themselves. This will lead to a significant change in material behavior, with respect to the previously discussed 90° specimens. With the load bearing capacity mainly being transferred to the fibers, it is to be expected that the flexural modulus of the material will increase drastically. This is due to the fact that the fibers can handle a lot more energy than the matrix itself before failure. Furthermore, their stiffness is much higher, which would mean that more force is required to deform them.

A higher amount of energy before failure can be absorbed by the fibers. This will lead to an increase in the surface area beneath the force-displacement curve. It can therefore also be assumed that either the flexural strength (related to the force at failure) and/or the deformation at failure (strain and deformation) will increase with these specimens in comparison to the 90° ones. The force displacement curve for the three point bending tests at room temperature of the 0° specimens is shown in figure 5.4.

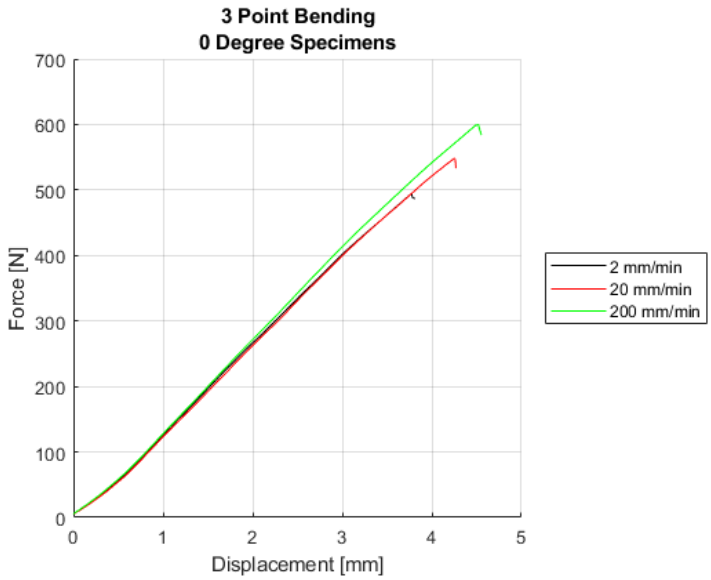

Figure 5.4: Force Displacement Curve of the 3 Point Bending Tests for 0° specimens at room temperature

Immediately, a large difference with the 90° specimens can be seen by looking at the pure shape of the graph. It is noticeable that the material behaviour is much more linear than that of the 90° specimens. This is due to the much more linear behaviour of the glass fibers with respect to the iPP matrix.

Secondly a significant increase in force (± 20 times higher than 90°) and displacement (± 3 - 4 times higher than 90°) at failure can be noticed. The numeric values for the material properties can be found in table 5.2 and are visually shown in figure 5.5.

Table 5.2: Properties of 0° specimens at different strain rates

Velocity [mm/min]	Strain Rate [s^{-1}]	Flexural Strain	Flexural Strength [MPa]	SEA [kJ/kg]
2	2.04e-4	0.0254	1212.1	0.7883
20	0.0020	0.0273	1344.8	1.1779
200	0.0128	0.0279	1424.6	1.2980

When looking at the trends shown in the table and figure, there are some key results noticeable. Firstly, there is once again no clear evidence for a relation between the modulus and strain rate. A more increasing trend is visible, but due to the range of errors, this is still not provable. The flexural

strength and deformation at failure both increase with an increasing strain rate. This is in line with the tensile properties of the material. The mentioned increasing trend in flexural strength and deformation at failure will automatically lead to an increase in specific energy absorption as shown in figure 5.5d.

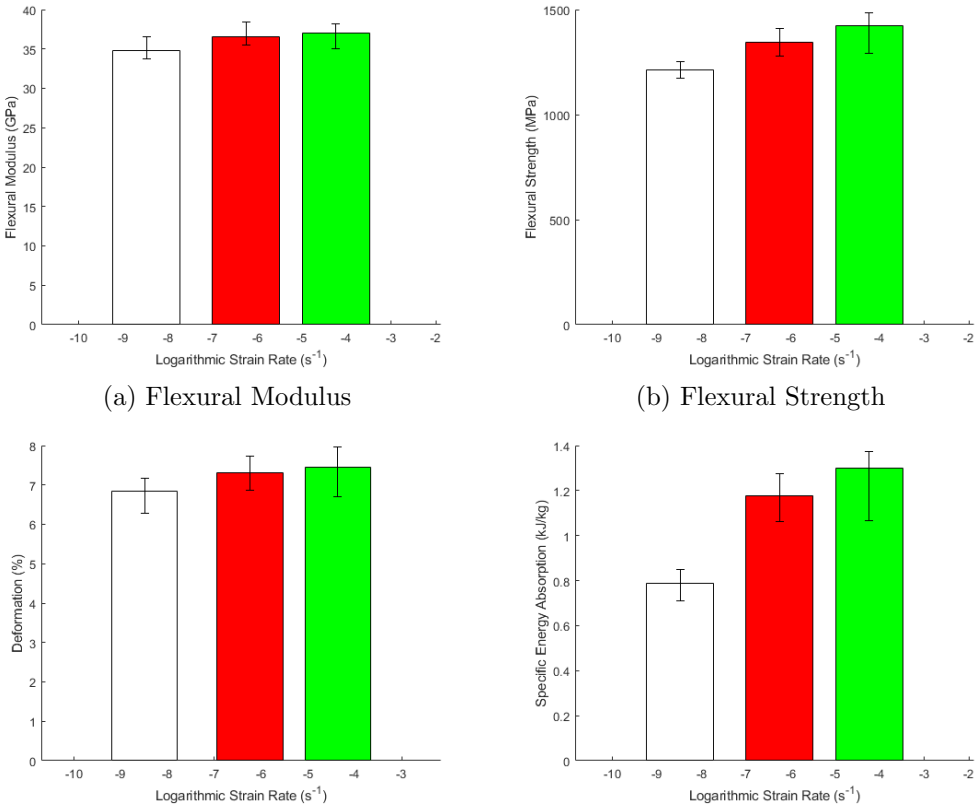

(a) Flexural Modulus

(b) Flexural Strength

(c) Deformation at failure

(d) Specific Energy Absorption

Figure 5.5: Mechanical Properties of 0° specimens at different strain rates

A look at the micrographs (as seen in figure 5.6) corresponding with the specimens tested with this quasi-static set-up shows that a similar trend between the different strain rate is once again noticeable. Large differences between the 0° and 90° specimens are also notable. Firstly, failure occurs on the compression - and thus impacted - side of the specimen. The failure behavior consists of matrix cracks and fiber fracture. Trendwise, an increase in strain rate will lead to an increase in affected area, both in depth and distance from the impacted region. This can be explained by the increased amount of energy absorbed by the specimen. Furthermore, the amount of fiber fractures increases with higher strain rates, which is in line with literature. Significant voids also exist at the higher strain rates, showing a larger amount of plastic deformation.

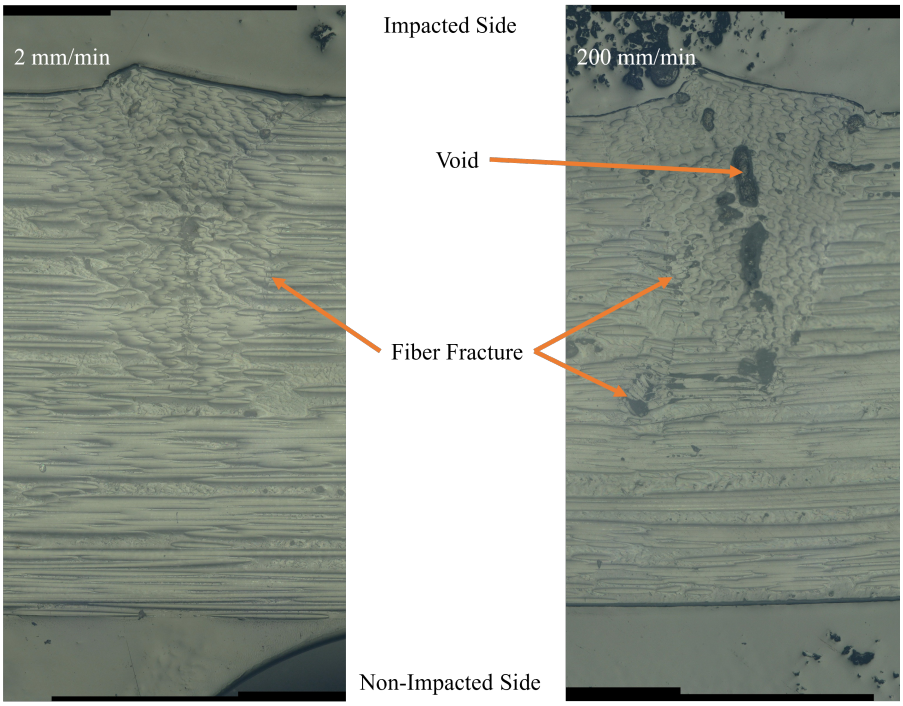

Figure 5.6: Micrographs [x300] of 0° specimens illustrating relation between strain rate and failure modes; 2 mm/min absorbed 0.7883 kJ/kg, 20 mm/min absorbed 1.2980 kJ/kg

5.2 Low Velocity Impact Testing

5.2.1 90° Specimens

Due to the load carrying responsibility of the matrix itself, the energy levels acquired via low velocity impact testing are more than likely high enough to cause terminal damage to the specimens. From the quasi static test cases, absorbed energy levels of around 0.02 J were achieved with partial failure. Given that the lowest impact energy level is set at 0.23 J, damage can be expected within the specimens.

Two different impact situations were evaluated. The force-displacement curves are shown in figures B.1 and B.2 in appendix B.1 The resulting data is presented in table 5.3 and figure 5.7. Herein, the dark green bars represent the data acquired from testing at 0.2336 J of impact energy and the dark blue bars represent that acquired from testing at 0.9347 J.

Table 5.3: Properties of 90° specimens at different impact energy levels

Impact Energy [J]	Strain Rate [s^{-1}]	Flexural Strain	Flexural Strength [MPa]	SEA [kJ/kg]
0.2336	2.9651	0.0137	58.3702	0.0181
0.9347	3.4137	0.0156	64.2734	0.0216

The acquired force-displacement curves show large oscillations, especially at the moment of impact. This was to be expected as Williams et al. [64] state that dynamic testing involves some well-known superimposed oscillations, especially at this moment of impact. This is also partly due to the oscillations which enter the system due to the impact itself, as proposed by Boria et al. [12]. Nevertheless, this makes using the slope-method as used before a little more challenging. On top of that, as mentioned in the methodology, the measured displacement values are step based and therefore difficult to fully examine.

All other properties show the expected trend of increasing at higher strain rates, except for the to-be expected independence of the modulus on the strain rate. This behavior was also found in the quasi static testing. One major issue is that the flexural values found in the low velocity impact testing are all much lower than those in the quasi static testing. This is a known issue and was found in

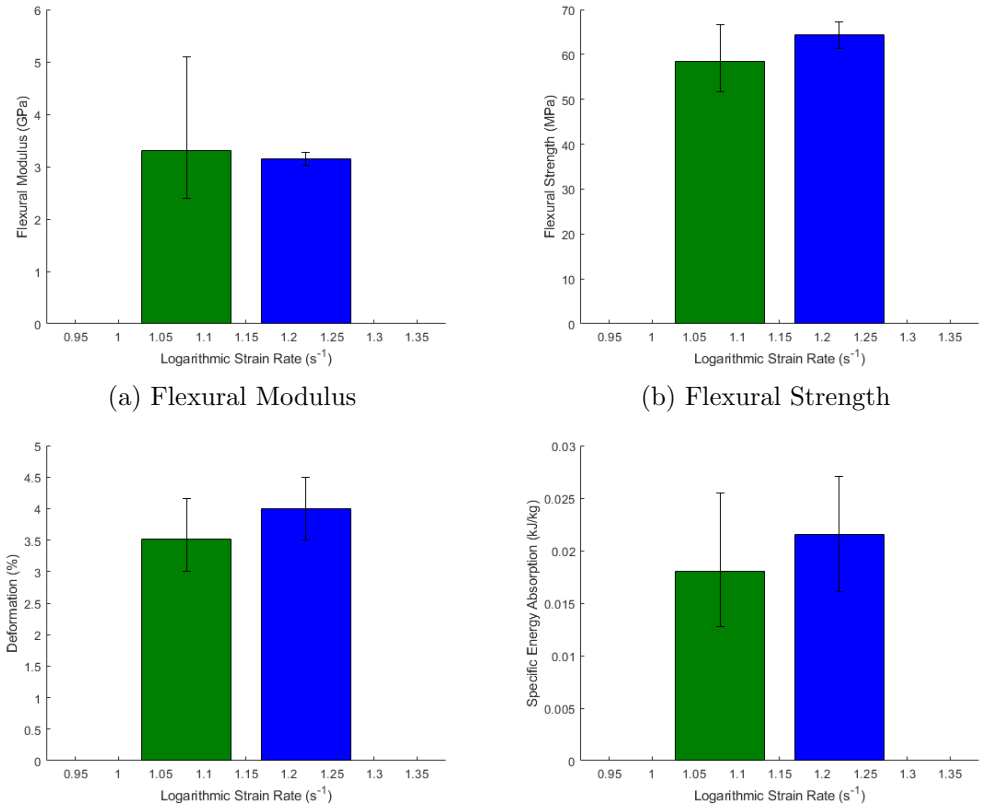

(a) Flexural Modulus

(b) Flexural Strength

(c) Deformation at failure

(d) Specific Energy Absorption

Figure 5.7: Mechanical Properties of 90° specimens at different impact situations

multiple studies - for all kinds of different materials -, as listed by Jacob et al. [34]. This will be further evaluated in section 5.4.

When looking at the micrographs of the impacted specimens - as shown in figure 5.8 -, there is one clear mode of failure present: a single matrix crack along the entire thickness. This was also as expected due to the nature of the specimens and based on the results found in the quasi-static testing (section 5.1.1). The crack growth initiated from the non-impacted side of the specimen, before growing throughout the thickness up until the impacted side. A clear split between the two halves of the specimen can be felt when examining the specimen. On the impacted side, a small layer of material is capable of holding both parts together. The difference in thickness for this small layer between the two impact situations is not distinguishable.

5.2.2 0° Specimens

From the quasi static test cases (see section 5.1.2), it was found that even at the lowest bending speed, the 0° specimens were able to absorb around 1.7 J of energy. This means that the used impact energy levels for the previously discussed 90° specimens would most likely cause no (external) damage to the specimens. One of these energy levels is still included in the measurements for verification purposes. 3 higher levels of impact energy are used to evaluate the material properties and failure behavior of the 0° specimens; 3.73 J, 14.92 J and 44.77 J.

The force-displacement curves can be found in figuren B.3 in appendix B.2. Accurately calculating the modulus is difficult due to the oscillations present in the system. The other properties can be calculated as per usual. The resulting data can be found in table 5.4 and figure 5.9. In the figure, the dark blue bars represents the tests executed at an impact energy level of 0.9281 J, yellow those at impact energy levels of 3.7325 J, cyan at 14.9201 J and burgundy at 44.7702 J.

The resulting trends are points of discussion. Firstly, the expected non-dependency of the modulus

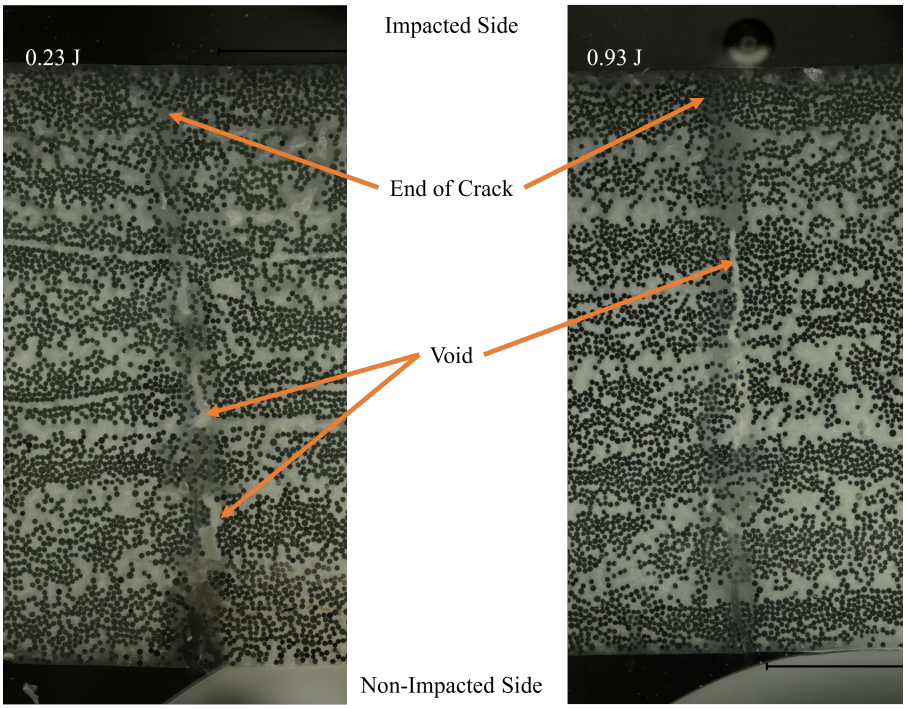

Figure 5.8: Micrographs [x300] of 90° specimens illustrating relation between strain rate and crack length; 0.23 J Impact Energy absorbed 0.0181 kJ/kg, 0.93 J Impact Energy absorbed 0.0216 kJ/kg

Table 5.4: Properties of 0° specimens at different impact energy levels

Impact Energy [J]	Strain Rate [s^{-1}]	Flexural Strain	Flexural Strength [MPa]	SEA [kJ/kg]
0.9281	1.8782	0.0273	864.4	0.0919
3.7325	3.6705	0.0440	1796.8	1.4154
14.9201	5.6133	0.0446	1771.9	2.0402
44.7702	7.0553	0.0479	1779.4	1.5818

on the strain rate is somewhat visible. Once again, due to the presence of the (in some cases large) errors, no definite conclusions can be drawn on this relation. It is clear that no extreme influence is noticeable when altering the strain rate. Hereby it has to be noted that in general, the differences in strain rate between the experiments are smaller than those measured in the quasi static cases.

In order to fully understand the material behavior and the graphs shown in figures 5.9b, 5.9c and 5.9d, one first has to look at the results on the individual energy levels. At the lowest energy level (0.9281 J, shown in dark blue) the impactor rebounds from the specimen without leaving any visual external damage. After further evaluation using an optical microscope, no significant internal damage was found. As a result, only 22.9% of the maximal impact energy was absorbed by the material. The abolsute values found for this impact energy level are therefore interesting on their own, but difficult to compare to the other energy levels.

When looking at the next energy level (that of 3.7325 J, shown in yellow), a very different story is presented. Herein, the impact situations resulted in significant visual damage to the specimens. Furthermore, these impacts led to an absorption of 87.7% of the possible maximal impact energy by the material. A very small rebound of both the crosshead and specimen was witnessed during testing, thus explaining some of the energy 'loss'. An interesting relation between failure modes and energy absorption can be made from these specimens, as will be discussed further on. This also includes their use in a comparison in material properties between levels of impact energy.

A similar story applies to the specimens which were evaluated at 14.9201 J (shown in cyan). The material properties of these specimens show the characteristic relations for the influence of strain

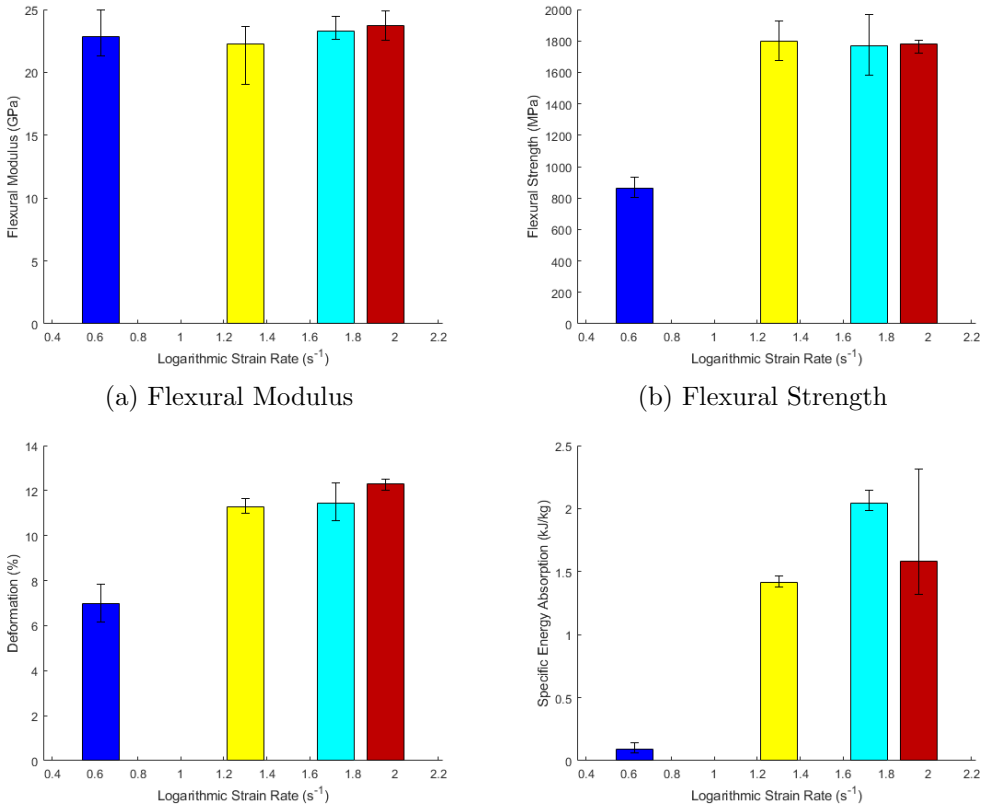

(a) Flexural Modulus

(b) Flexural Strength

(c) Deformation at failure

(d) Specific Energy Absorption

Figure 5.9: Mechanical Properties of 0° specimens at different impact situations

rate, with respect to the previously mentioned energy level. An interesting note to make is that the amount of energy absorbed by these specimens is higher than that of the previously mentioned samples (4.7180 vs. 3.2732 J, respectively), although a much smaller amount of the impact energy is actually absorbed by the material (31.6% vs. 87.7%). This will lead to the assumption that the material in this shape/structure has reached its absorption limit (as also explained by Aktas et al. [1]) at around 2.1 kJ/kg. This is arguable since the possible maximal impact energy level of the previous test was lower than the amount of energy absorbed by these specimens.

Both of the aforementioned groups of specimens show some similar failure behavior but the main difference is the presence of clearly visible plastic deformation at the higher energy level. When looking at the micrographs in figure 5.10, many comparable types of failure are visible, especially delaminations, matrix cracks and fiber fracture. The specimen subjected to 14.92 J of impact energy has damage visible throughout the entire thickness, whereas the specimen subjected to 3.73 J has a small piece that is still intact. What is noticeable in comparison to the found results in the quasi static cases is the lack of visible flexural damage on the non-impacted side (top side in the figure). In the quasi static cases, a large 'bulk' of material formed on the flexural side, whereas these seem to be lacking in these low velocity impact tests.

The last case to be discussed are the specimens tested at a theoretical maximal impact energy level of 44.7702 J. Given that the specimens tested at 14.9201 only absorbed a small amount of the total energy of the impact, it is to be expected that a similar case happens at higher levels of impact energy. This turned out to be the case as the specimens only absorbed 3.65 J of energy (8.2% of the total impact energy). A massive rebound of the impactor, along with the introduction of a large velocity into the specimen itself allowed for this small 'useful' energy transfer.

A similar behavior to the specimens tested at 3.73 J is found when looking at the micrographs. However, it appears as if the energy absorption happens in a more random way. Some of the specimens analysed showed signs of flexural deformation (on the non-impacted side) with smaller amounts of

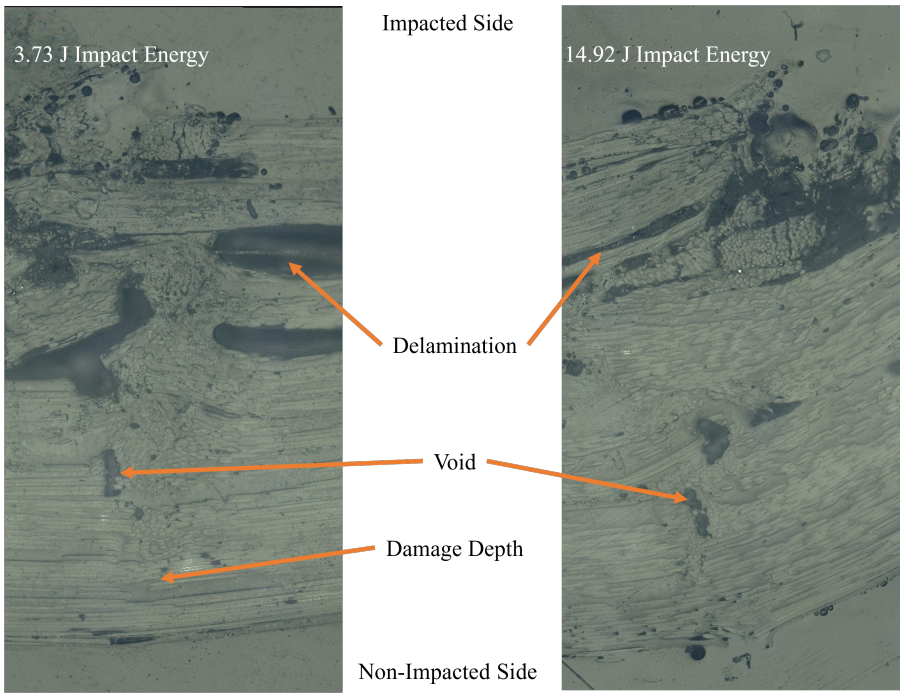

Figure 5.10: Micrographs [x300] of 0° specimens illustrating relation between strain rate and failure modes/depth of failure; 3.73 J Impact Energy absorbed 1.4154 kJ/kg has not fully failed, 14.92 J Impact Energy absorbed 2.0402 kJ/kg shows damage up until the non-impacted side

delamination, which was not the case in the 3.73 J sample group. Others showed more delaminations but without the increased flexural failure or plastic deformation. Hereby it has to be noted that some of the samples were impacted a second time during the testing cycle, before being bounded away from the supporting cylinders.

Concluding, there is a great dependency on the failure behavior of the 0° specimens under impact situations. This also applies to the material properties of the composite under these conditions. Adding to that, there is no ideal transfer of energy between the impactor and specimens. This will also influence the found results.

It is of great value to keep the different zones of the energy profiling method, as proposed by Aktas et al. [1], in mind when evaluating the data found in this section. Firstly, no damage is present at impact energy levels of ≤ 0.93 J. No specific study has been done on the penetration transition point (the energy level at which both internal and external failure starts to occur), but this can be extremely useful in future work. A further elaboration on this can be found in section 7. The found results imply a maximal specific energy absorption capability of around 2.1 kJ/kg for this material in its current structure and shape. As mentioned before, these both have a great influence on the energy absorbing capability of a material.

The expected trends corresponding with the material properties and strain rate dependency hold within the zone in which energy absorption is also increasing with increasing impact energy/strain rate, the penetration zone as described by Aktas et al. This leads to the conclusion that the material properties are related to the strain rate but governed by a range of impact energy.

5.3 Low Temperature Quasi-Static Testing

5.3.1 90° Specimens

A significant part of the load transmitted to the transverse specimens is carried by the polymer itself. It is therefore expected that the influence of the polymer on the results of these experiments is large. For this type of experiments, this is of extra importance due to the change in temperature and the effect of the temperature on the properties of the polymer itself. Figure 5.11 shows the mechanical properties of the 90° specimens at different temperature levels. The red bars represent the results at 20° C (room temperature), light blue 0° C, olive −15° C and magenta −30° C. All data is also presented in table 5.5

Hussain et al. [32] found that Isotactic Polypropylene has a glass transition temperature of 8.0° Celcius. Furthermore, they state that one of the major drawbacks of PP is its brittleness at low temperatures, especially beneath the glass transition temperature. This was also stated by Strobl [55] and Kumar [40]. Given that the used temperature levels are all beneath the glass transition temperature, it can be expected that the deformation at failure will decrease with a decrease in temperature. This is contradictory to the results found in the room temperature testing in section 5.1.1, which showed an increase in deformation at failure with an increase in strain rate.

In figure 5.11c, it can be seen that this expectation is indeed verified by the experiments. A decrease in temperature leads to the predicted decrease in deformation at failure, due to the increase brittleness of the polymer.

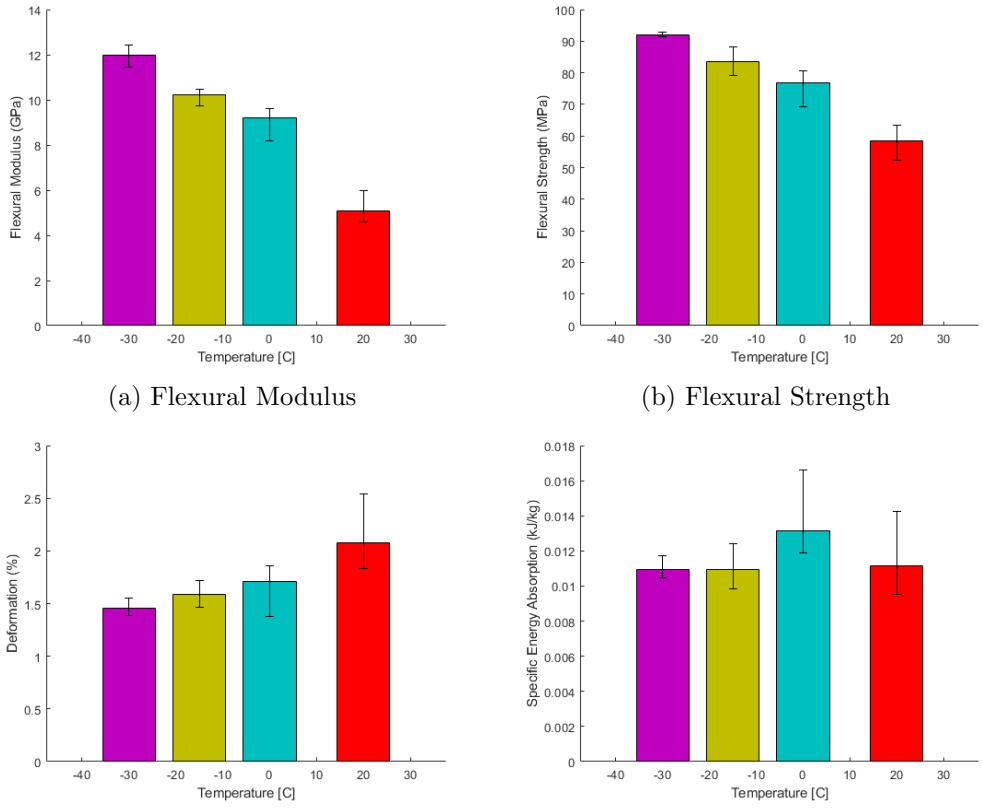

(a) Flexural Modulus

(b) Flexural Strength

(c) Deformation at failure

(d) Specific Energy Absorption

Figure 5.11: Mechanical Properties of 90° specimens at different temperatures

From the graphs, a number of conclusions can be drawn. In figure 5.11a, a large increase in modulus at lower temperatures can be distinguished. This is in line with what Govaert and van der Vegt [61] mention. They state that, for a large number of polymers which turn brittle at low temperatures, the modulus increases at these lower temperatures. This also reinstates the larger influence of temperature on the polymer behaviour, similar to the decrease in deformation (fig 5.11c) at failure as mentioned

Table 5.5: Properties of 90° specimens at different temperatures

Temperature [°C]	Strain Rate [s^{-1}]	Flexural Strain	Flexural Strength [MPa]	SEA [kJ/kg]
20	0.0017	0.0078	58.3932	0.0112
0	0.0017	0.0064	76.5584	0.0131
-15	0.0017	0.0060	83.6775	0.0110
-30	0.0017	0.0055	93.0326	0.0109

before.

The increase of flexural strength at lower temperatures (fig 5.11b) follows the results found in the room temperature testing, i.e. an increase in strain rate leads to an increase in flexural strength of the material.

Finally, the specific energy absorption shown in figure 5.11d shows a near independence to the temperature/strain rate. This is caused by the increased brittleness of the material at lower temperatures. The increase in strength due to the higher strain rates is countered by the decreased deformation, thus removing a lot of the energy storing capability due to deformation.

This trend is also visible when looking at the micrographs (fig 5.12) of the failed specimens. Due to the increased brittleness and strength, the final crack size is shortened at lower temperatures. All showed the presence of a crack only within the matrix and no signs of fiber or fiber-matrix bonding related damage. This is in accordance with the results found in the room temperature testing. The amount of energy which is absorbed by the material is simply not enough to cause any other failure mode than matrix cracking. The crack propagation is the only sign of the different temperatures/simulated strain rates applied to the specimens when looking at optical microscopy results. The use of a SEM can prove more brittleness, as proposed before.

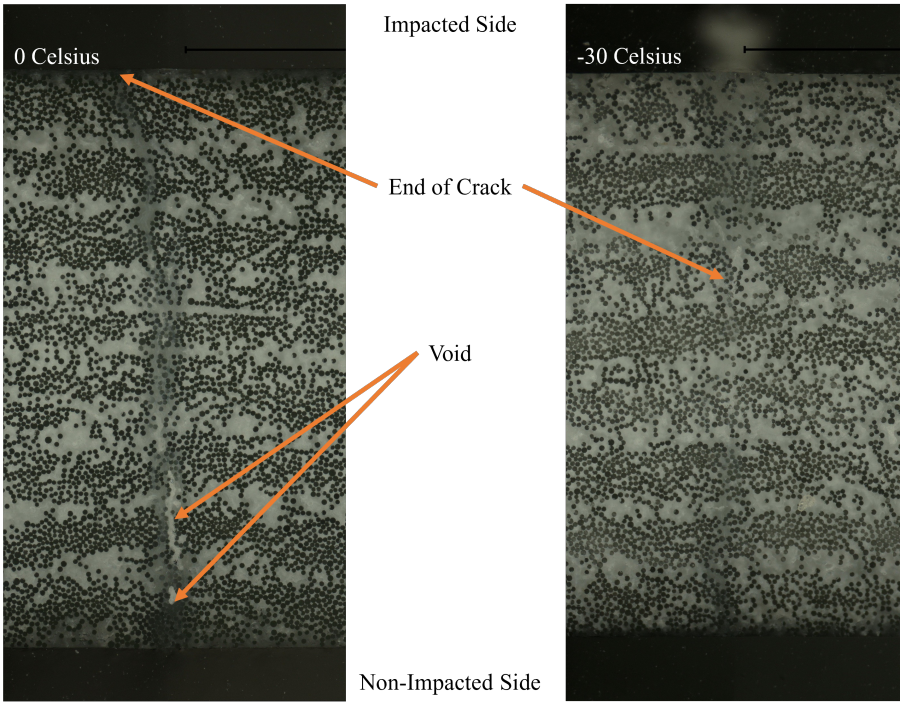

Figure 5.12: Micrographs [x300] of 90° specimens illustrating relation between strain rate and crack length; Specimen tested at 0° Celsius absorbed 0.0131 kJ/kg, tested at −30° Celsius absorbed 0.0111 kJ/kg

5.3.2 0° Specimens

The 0° specimens material behaviour is much more reliant on the properties of the fibers than that of the polymer itself. The massive influence that the temperature has on the results of the experiments conducted with the transverse specimens therefore is not expected with these specimens. A similar trend in results with respect to the quasi static testing at room temperature is expected.

Similar to section 5.3.1, the red bars in figure 5.13 represent the results of tests at 20° C, light blue 0° C, olive −15° C and magenta −30° C. The data is also presented in table 5.6.

Table 5.6: Properties of 0° specimens at different temperatures

Temperature [°C]	Strain Rate [s^{-1}]	Flexural Strain	Flexural Strength [MPa]	SEA [kJ/kg]
2	0.0019	0.0281	1344.8	1.1779
20	0.0020	0.0319	1549.9	1.3171
-15	0.0020	0.0413	1883.4	1.8850
200	0.0020	0.0436	1917.4	2.1725

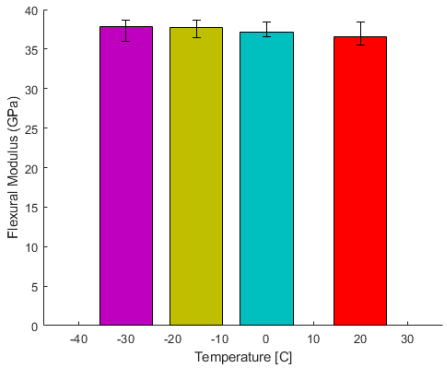

(a) Flexural Modulus

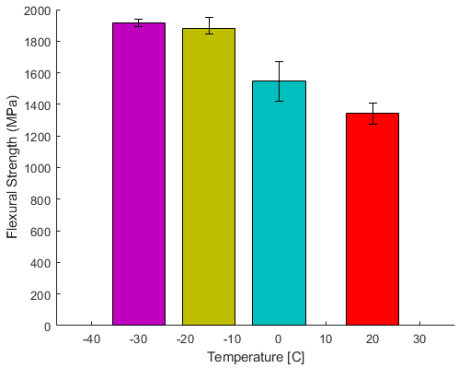

(b) Flexural Strength

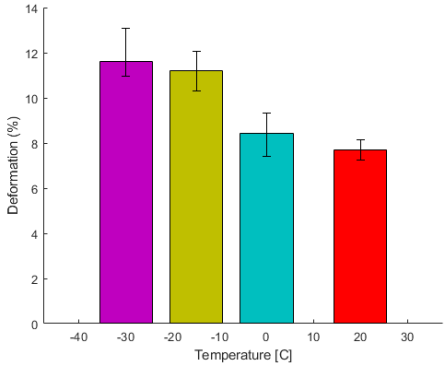

(c) Deformation at failure

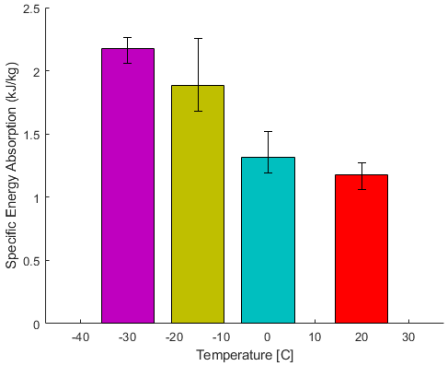

(d) Specific Energy Absorption

Figure 5.13: Mechanical Properties of 0° specimens at different temperatures

In the room temperature testing (section 5.1.2), it was shown that there was no real relation between the modulus of the composite and the applied strain rate. As shown in figure 5.13a, this behaviour also applies to any temperature differences. A very slight increase in modulus at lower temperatures can be distinguished, but due to the presence of the overlapping errors between all results, this conclusion cannot be properly drawn.

Increases in flexural strength and deformation at failure at lower temperatures are definitely present. These trends also follow up to the ones found in the room temperature testing of section 5.1.2. Due to these combined increases, an increasing trend in specific energy absorption capability at lower temperatures follows suit. This, once again, is in line with expectations and previously discussed results.

When looking at the micrographs (figure 5.14), large differences between the different temperatures can be seen. These mainly include a large range of affected damage zones within the specimens, but there are also different failure modes that affect some of the specimens. The most obvious one is the presence of delaminations, which do not occur in the specimens tested at 20 and 0 ° C and are present in the specimens tested at -15 and -30 ° C. This is in line with the results found in the low velocity impact testing, i.e. the presence of delaminations proves a larger amount of absorbed energy/delaminations come to exist if higher energy levels need to be absorbed.

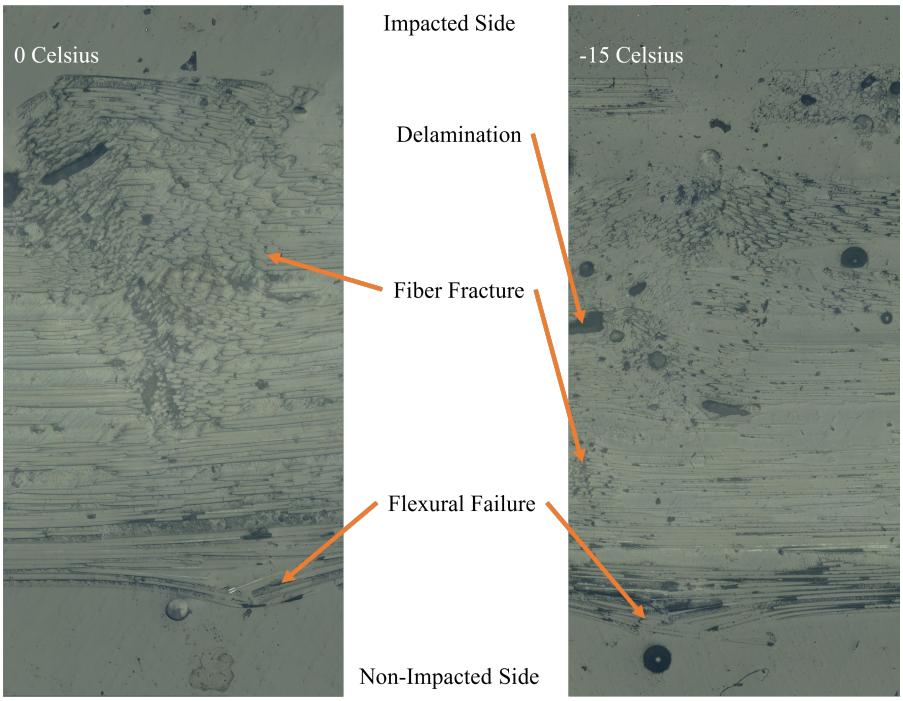

Figure 5.14: Micrographs [x300] of 0° specimens illustrating relation between strain rate and failured modes; Specimen tested at 0° Celsius absorbed 1.3171 kJ/kg, tested at −15° Celsius absorbed 1.8850 kJ/kg

Another thing to notice is the presence of failure throughout the entire thickness of the specimen. Damage propagation is visible throughout the entire thickness of the material, with a sort of bump forming on the other side of the impacted region. This flexural failure is not present in the quasi-static testing at room temperature (figure 5.6 in section 5.1.2).

All samples show signs of matrix cracking and fiber breakage. Once again, the severity of the failure modes and the region they affect is highly dependent on the temperature/simulated strain rate. As a rule of thumb, the higher the (simulated) strain rate, the larger the affected area and the more severe the symptoms of the failure modes.

To conclude, the unidirectional specimens tested at lower temperatures show similar trends to those tested at room temperature and different strain rates. Lower temperatures lead to larger amounts of energy can be absorbed by the specimens, which also causes a major difference in failure behaviour. Most noteworthy is the introduction of delaminations at lower temperatures/higher absorbed energy levels.

5.4 Comparison Research Methods

This thesis combined three different research methods to analyze the short term behavior of a thermoplastic composite. In the previous sections, the individual results were discussed. To fully underline the relations between the different methods used, a comparison is required. This section focuses on the relations between the used research methods and questions the possibility of using the proposed combination to fully define the material behavior within a specified range of strain rates.

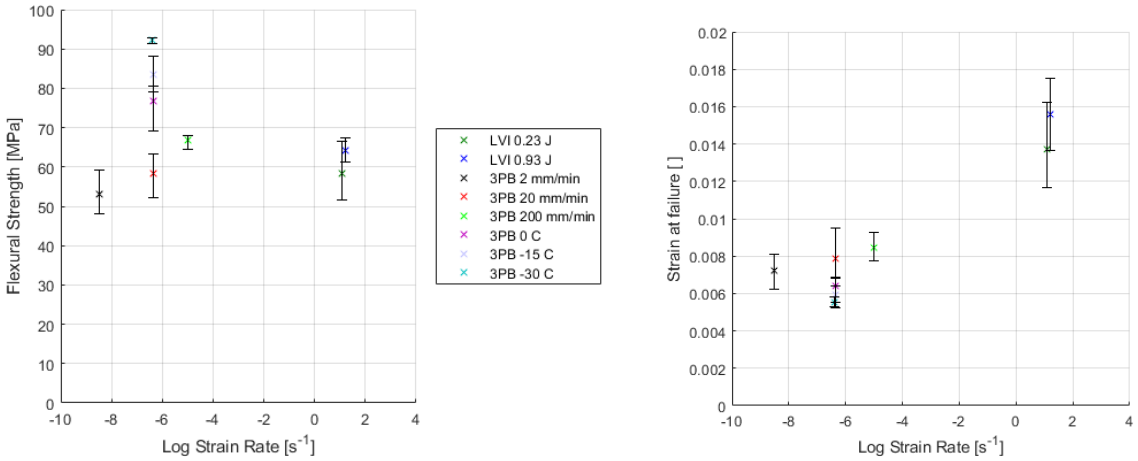

(a) Flexural Strength

(b) Strain at failure

Figure 5.15: Differences in research methods for 90° specimens

Figure 5.15 shows the relation between the flexural strength, strain at failure and strain rate for all three research methods for the 90° specimens. Individual results showed a constant increase in flexural strength at failure with increasing strain rate. The increasing trend is visible when looking at all quasi-static tests (both room temperature and at lowered temperatures). The data for the lowered temperature tests is located on the same strain rate as the room temperature three point bending as the measured data corresponds with the set 20 mm/min displacement.

The massive influence of the temperature on the material properties is also visible in figure 5.15. The strain at failure decreases drastically at lower temperatures whereas the trend (both in room temperature quasi-static and low velocity impact testing) is increasing at increasing strain rates. This is all due to the increased brittleness at lower temperatures.

It is interesting to note that the average values for the flexural strength found in low velocity impact testing are somewhat lower compared to the quasi-static tests. This is due to the large deviations found in LVI. Accurately positioning the drop weight as well as slight changes in contact between the impactor and specimen are to blame for this.

As previously mentioned in section 5.2.1, the calculation for the modulus was difficult due to the oscillations present within the results. Since there is no clear relation between the strain rate and modulus (only the large temperature influence), it is assumed that these values are the results of the complex calculations.

The different research methods all show promising and comparable behavior for the 0° specimens. Figure 5.17 shows the relation between the absolute strength, strain at failure and strain rate for these specimens. Both properties show the expected behavior and the trends can be continued throughout all methods. This is especially important as the flexural strength trend based on the quasi-static tests also holds for the low velocity impact tests. The one exception - which has been extensively discussed in section 5.2.2 - is the 0.93 J Impact Energy tested sample group. This is due to the impact energy level being too low to create internal and external damage, thus rebounding of the specimen while transferring only a small amount of energy.

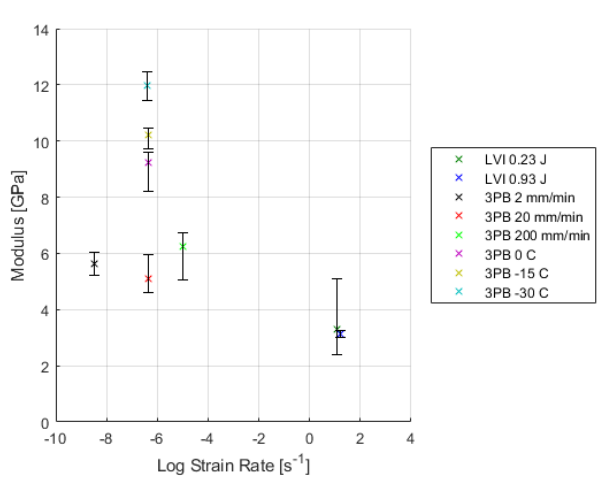

(a) Flexural Modulus

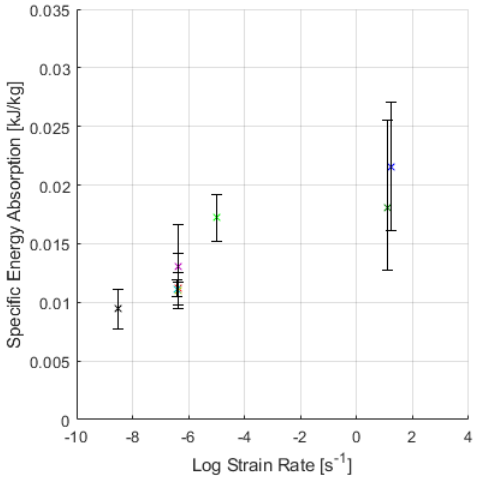

(b) Specific Energy Absorption

Figure 5.16: Differences in research methods for 90° specimens

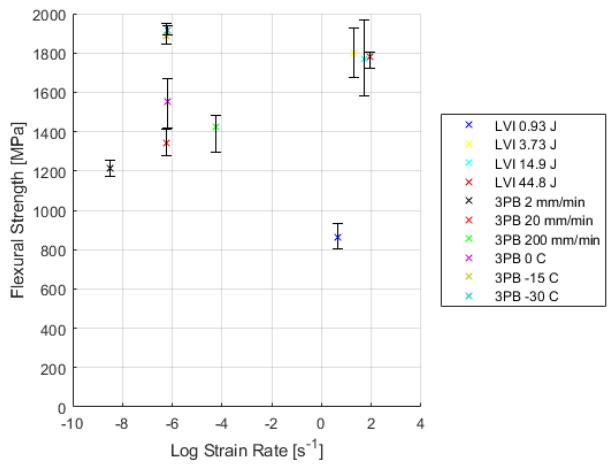

(a) Flexural Strength

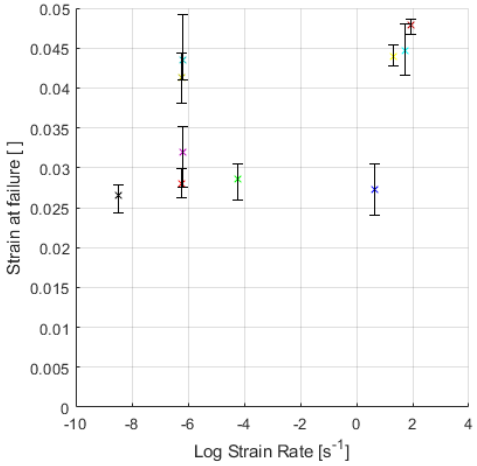

(b) Strain at failure

Figure 5.17: Differences in research methods for 0° specimens

This energy transfer is also visible in figure 5.18, as the absorbed energy is much lower than that found in all other sample groups. Once again, the trends can be continued throughout the different research methods. One thing to note here is that - when also looking at figure 5.17 - it is quite unclear which test has reached a higher strain rate. The low velocity impact testing and low temperature quasi-static test results show similar behavior. This was also noticed in the micrographs of both testing methods. This would lead to the assumption that the testing methods are comparable and operate at similar strain rates.

It can be concluded that the combination of the three proposed testing methods can be used together for the 0° specimens. For the 90° specimens, it is advised to only use room temperature testing at different strain rates to compare the resulting material properties as these specimens are highly temperature dependent. There are some important points to note when combining the different methods into a single research output. Especially for thermoplastic materials which rely heavily on the load bearing capacity of the polymer itself, the fracture toughness can be heavily influenced by the strain rate, thus yielding absolute lower values for low velocity impact testing. Secondly, due to the nature of the test, three point bending tests will always lead to failure, low velocity impact testing requires a minimal amount of impact energy before failure occurs. Data gathered with lower values of impact energy, which only lead to rebounding of the impactor, cannot be compared to data found for

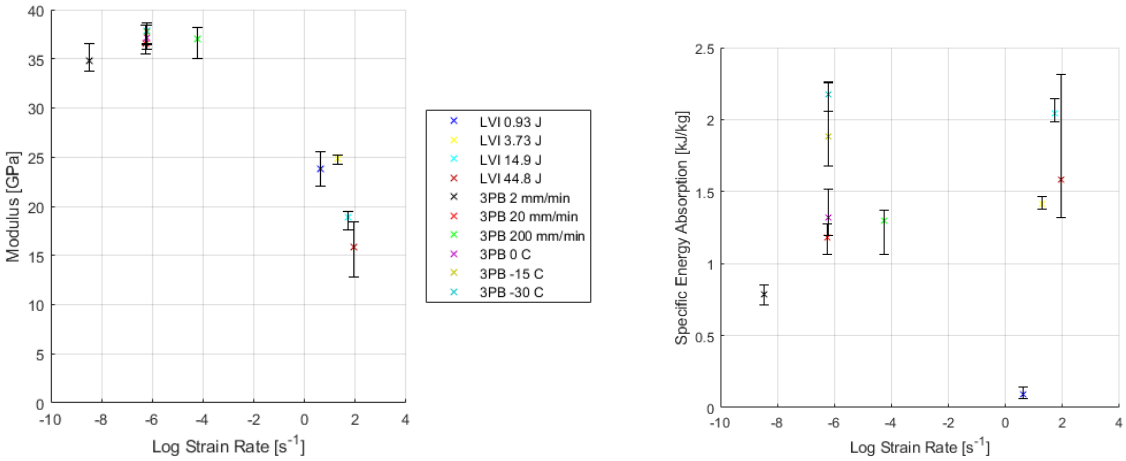

(a) Flexural Modulus

(b) Specific Energy Absorption

Figure 5.18: Differences in research methods for 0° specimens

damaged and failed specimens.

Chapter 6

Conclusions

In section 2, 4 research goals were stated. Due to the limited time-span and ever-enlarging possibilities, it was not possible to conclusively answer all goals. This research did however find a lot of answers and data suitable for further evaluation which will be concluded and summarized in this section. In the following section, a detailed explanation into possible future work with respect to answering the here set research goals is given.

The main goal was to gather data to create a predictive model for the behavior of glass-fiber reinforced isotactic polypropylene under impact situations. The most important factor here are the results gathered in the low velocity impact testing. However, the range of different strain rates tested is limited (all between 10^0 and $10^1 s^{-1}$). Therefore, the addition of quasi static three point bending testing (at strain rates between 10^{-4} and $10^{-2} s^{-1}$) was necessary to create a more usable data set. For comparability, the low velocity impact tests were designed to mimic the conditions of the quasi static tests.

Quasi-static testing at lower temperatures was included to provide information on the material response to temperature change. This is also a starting point for the investigation into the possible use of the time-temperature-superposition principle (see section 7) to investigate strain rates that cannot be tested with the current set-ups.

All tests were executed with the same specimen dimensions (60 x 11.75 x 2 mm), with unidirectional fiber reinforcements in the material. The pre-made sheets were cut in such a way that the specimens were tested at either 0 or 90° angles with respect to their fiber direction.

- **1: Identify the influence of fiber direction on the material properties and failure behavior.** The fiber orientation has a large influence on the material properties of the composite, independent of the used research method and strain rate. 0° specimens showed moduli which were up to 6 times higher, an absolute strength up to 20 times higher and a strain at failure of 2 to 8 times higher than in 90° specimens.

  The failure behavior of the material is also highly dependent on the fiber orientation. 90° specimens showed failure propagation from the non-impacted side of the specimens whereas 0° specimens showed failure propagation from the impacted side. 90° specimens failed purely on matrix failure, in all cases the forming of a single crack which propagates throughout the material. The 0° specimens failed by a number of failure modes, if enough energy was introduced into the system, with matrix cracking occurring at all strain rates. With increasing strain rates/energy levels, fiber fracture and eventually delaminations were found.

- **2: Identify the relation between the strain rate and the stiffness, strength and strain at failure of thermoplastic composites under impact loading** For both the 0 and 90° specimens, there is a significant relation between the properties/failure behavior and the applied strain rate/energy level. Contradictory, a general independence of the flexural modulus

of the material on the strain rate was measured by all test methods, for both types of specimens. There is one exception to this, which will be discussed further on.

The absolute strength of the material at failure showed an consistent increasing trend with increasing strain rate/energy level (or decrease in temperature). This was found to be true for all executed tests.

The deformation at failure (strain at failure) followed the same pattern. An increase in strain rate or energy level would lead to an increase in its value. A single exception to this is during the quasi static tests at lower temperature for the 90° specimens. These showed a decreasing trend with a decrease in temperature (increase in mimicked strain rate). This is due to the tests being executed below the glass transition temperature of the material. Polypropylene is known to become extremely brittle at low temperatures, which was proven by the experiments. Simultaneously, its modulus (the aforementioned exception) increases drastically at lower temperatures, this was also shown in the experimental data. This behavior was not found in the 0° specimens, due to the load bearing capacity being on the much less temperature dependent glass fibers.

This brittleness at low temperatures also influences the specific energy absorption capability of the material. For all tests, it was shown that this increases with an increase in strain rate/energy level. Due to the brittleness, this is not the case for the 90° specimens tested at lowered temperatures. The specific energy absorption capability of the material is hardly influenced by the temperature because of the interaction between the increased modulus and decreased strain at failure.

- **3: Identify the failure modes of thermoplastic composites under impact loading and their energy absorbing behavior** All 90° specimens showed similar failure behavior in the form of a single matrix crack along the entire width of the specimens. The specimens started cracking due to the flexural stress on the non-impacted side of the specimen. The amount of energy absorbed by the specimen was highly influential on its length with respect to the thickness of the material. Only the specimens evaluated after impact testing showed a full rupture (crack throughout the entire thickness). For the others, a relation between the crack depth and absorbed energy can be made.

  All 0° specimens have failure at the impacted side of the specimen, if the applied energy is sufficient to cause both internal and external failure (the mimimal absorbed energy level which caused this was measured at 0.78 kJ/kg). Large differences between the different tests were discovered. Matrix cracks and small amounts of fiber fracture were noticed at low energy level. An increase in strain rate leads to an increase in affected area, both in terms of depth and distance to the impacted location. Furthermore, this leads to the introduction of delaminations within the material (starting at 1.3 kJ/kg). Again, higher energy levels and strain rates leads to further growth of these delaminations, in both number and distance from the impacted zone.

- **4: Correlate the low velocity impact with high strain rate quasi-static bending** The found trends are nearly all equal, independent of the testing method. This is promising as it allows the use of any of the discussed testing methods to be used for rate-dependent testing. However, the Low Velocity Impact testing is quite volatile and will yield differentiating results. As long as that is taken into account, both methods can work in unison.

  The use of the time-temperature-superposition principle (see secion 7) is questionable. Firstly, for the 0° specimens, results showed a promising similar trend to tests at room temperature and different strain rates. The addition of further testing at different temperatures and strain rates can provide useful information on the material behavior over a large range of strain rates. On the other hand, the 90° specimens were severely influenced by the temperature change, becoming much more brittle and stiff. Although important to understand, the use of the time-temperature-superposition principle for mimicking strain rates is not possible for these specimens.

All in all, this thesis has provided a valuable amount of data for the creation of a predictive model for the short term failure behavior of thermoplastic composites. The large influence of the fiber direction in unidirectional samples has been investigated. Trending relations between the strain rate and the modulus, flexural strength and strain at failure were found for flexural testing. The possibility of the use of the time-temperature-superposition principle was explored, but will require some more attention in further studies. Relations between the different failure modes occurring at different strain rates and impact situations were investigated. Finally, the use of low velocity impact testing and quasi-static three point bending testing were combined and compared to provide a correlation.

Chapter 7

Recommendations

The main research goal of this thesis is to create predictive models for the use of thermoplastic composites in the automotive industry. This is a very broad and extensive goal, which cannot be fully achieved given the small timespan of this project. To achieve this goal, a number of recommendations is given on possible future work and/or alterations to the work done in this thesis.

- Identifying the influence of material thickness on the material properties/failure modes. In this thesis, the crack or failure propagation throughout the thickness of the used specimens was an important part in demonstrating the amount of energy absorbed. Thicker (or thinner) specimens can lead to completely different material behavior. Jacob et al. [34] concluded in a literature review that there is an ideal range of material thickness (in ratio with the other dimensions) for which materials absorb the highest amount of energy. Anything above or below this range will lead to a decrease. Finding this range can be of great importance for the modeling.
- Identifying the influence of the shape/structure on the material properties/failure modes. Flat specimens were used in this thesis, Falzon et al. [26] and Dubey and Vizzini [23] noticed large influences of the shape on the properties and failure. Dubey and Vizzini noted a 12% decrease in absorbed energy per unit mass for flat specimens with respect to tube specimens under quasi-static compression testing. They conclude that the flat plates can be used as cheap alternatives during testing before using that data in simulations. Given that these tests were for a graphite/epoxy composite, it is useful to do them for this material as well.
- Using different lay-ups and fiber directions. All specimens used in this thesis came from plates with 8 layers of unidirectional fibers. Since they were cut differently, the effect of the fiber orientation could be determined. However, no testing was done on 45° unidirectional fibers and on possible lay-ups which combine fiber directions. Given the large influence of the fiber direction on the properties and failure modes, this is of interest when creating a predictive model.
- Combining the results of this thesis with tensile, shear and compression testing. The relation between the found results for the flexural/impact and tensile testing has been discussed partly in this thesis. However, to fully understand the material behavior, one has to look at compression and shear as well. Boria et al. [11] executed a combination of all the aforementioned tests on polypropylene reinforced with more polypropylene fibers. This can provide insightful information into the material behavior under different circumstances.
- Using the Time-Temperature Superposition principle to relate the data found for temperature dependent testing to strain rates. In order to investigate the material behaviour in the strain rate range gap between the strain rates that can be achieved with quasi static testing (between 10^{-4} and $10^{-2}s^{-1}$) and those in impact testing (between 10^{0} and $10^{1}s^{-1}$), quasi static testing at lower temperatures should be executed. This mode of testing will allow for the replication of behaviour at higher strain rates while testing can take place at easily achievable strain rate ranges for the used equipment.

To fully understand this behaviour, one has to look into the effect of temperature on the material behaviour. This effect is described by the Arrhenius equation 7.1 on a molecular level. Herein, τ is the relaxation time of the process. Combining this with frequently used models for the visco-elastic behaviour of polymers, it is possible to rewrite this equation to describe this relaxation time in terms of the materials viscosity as well as the process time - in stead of its temperature -, as seen in equation 7.2. Hereby it has to be noted that the spring constants E_i are assumed to be temperature independent.

$$\tau = c \cdot exp(\Delta U/kT) \tag{7.1}$$

$$\tau_i = \frac{\eta_i}{E_i} = \frac{c_i^{'}}{E_i} exp(\Delta U/kt) \tag{7.2}$$

These relations imply that there is a direct relation between the temperature at which a material is deformed and the timespan over which it is tested. This is called Time-Temperature-Superposition, as described by Govaert and van der Vegt [61]. They state that a change in temperature (from T_0 to T) will lead to a shift of the modulusgraph over the log t-axis. This shift can be described by equation 7.3, in which α_T is defined as shown in equation 7.4.

$$ln(\alpha_T) = \frac{\Delta U}{k} \cdot \left(\frac{1}{T} - \frac{1}{T_0} \right) \tag{7.3}$$

$$\alpha_T(T) = \frac{\tau_i(T)}{\tau_i(T_0)} \tag{7.4}$$

Changing the temperature at which experiments take place can therefore largely influence its results. It hereby has to be noted that the actual strain rate at which testing occurs does not change, the material will solely behave as if under the influence of a different strain rate. In practice, an increase in temperature will lead to an effect similar to that of lower strain rates, whilst lowering the temperature will lead to an effect similar to that of a higher strain rate. The latter of these will be used to 'fill' the gap between the two proposed methods of testing by using quasi static tests at lowered temperatures to simulate the behaviour at higher strain rates.

This can be done by testing at the already presented temperatures at different strain rates to create the master graph of the modulus with respect to the log time. After this, the found data can be combined to the appropriate mimicked strain rate. During the thesis, it was found that the method could prove very useful for 0° specimens given their similar response to lower temperatures as to higher strain rates in room temperature testing. For 90° specimens, attention is required as those proved to be highly temperature dependent and become much more brittle at lower temperatures.

Bibliography

[1] Mehmet Aktas, Cesim Atas, Bülent Murat Icten, and Ramazan Karakuzu. An experimental investigation of the impact response of composite laminates. *Composites Structures 87*, pages 307–313, 2009.

[2] B. Alcock, N.O. Cabrera, N. M. Barkoula, and T. Peijs. Low velocity impact performance of recyclable all-polypropylene composites. *Composites Science and Technology, 66*, pages 1724–1737, 2006.

[3] Yoshihiko Arao, Norihiko Taniguchi, Tsuyoshi Nishiwaki, Norio Hirayama, and Hiroyuki Kawada. Strain-rate dependence of the tensile strength of glass fibers. *Journal of Materials Science*, 47:4895–4903, 06 2012.

[4] D.R. Askeland and W.J. Wright. *The Science and Engineering of Materials, Enhanced, SI Edition.* Cengage Learning, 2015.

[5] Aswani Kumar Bandaru, Shivdayel Patel, Suhail Ahmad, and Naresh Bhatnagar. An experimental and numerical investigation on the low velocity impact response of thermoplastic hybrid composites. *Journal of Composite Materials, 52(7)*, pages 877–889, 2018.

[6] F. Barthelat and H. Lobo. High velocity 3 point bending test using an impact tower 906, annual technical conference; 58th, society of plastics engineers. In *TECHNICAL PAPERS OF THE ANNUAL TECHNICAL CONFERENCE-SOCIETY OF PLASTICS ENGINEERS INCORPORATED, Society of Plastics Engineers, Annual technical conference; 58th, Society of Plastics Engineers*, volume 3, pages 2961–2964. SPE;, 2000.

[7] M.A. Basith, N.C. Reddy, S. Uppalapti, and S.P. Jani. Crash analysis of a passenger car bumper assembly to improve design for impact test. In *Materials Today: Proceedings*, 2020.

[8] Gareth W. Beckermann and Kim L. Pickering. Mode i and mode ii interlaminar fracture toughness of composite laminates interleaved with electrospun nanofibre veils. *Composites Part A: Applied Science and Manufacturing*, 72:11–21, 2015.

[9] M. L. Benzeggagh and S. Benmedakhene. Residual strength of a glass/polypropylene composite material subjected to impact. *Composites Science and Technology, 55*, pages 1–11, 1995.

[10] Andrzej Bledzki, P. Franciszczak, and Agnieszka Meljon. High performance hybrid pp and pla biocomposites reinforced with short man-made cellulose fibres and softwood flour. *Composites Part A: Applied Science and Manufacturing*, 74, 07 2015.

[11] S. Boria, A. Scattina, and G. Belingardi. Experimental evaluation of a fully recyclable thermoplastic composite. *Composites Structures 140*, pages 21–35, 2016.

[12] S. Boria, A. Scattina, and G. Belingardi. Impact behavior of a fully thermoplastic composite. *Composite Structures, 167*, pages 63–74, 2017.

[13] W.J. Cantwell and J. Morton. Geometrical effects in the low velocity impact response of cfrp. *Composite Structures 12*, pages 39–59, 1989.

[14] W.J. Cantwell and J. Morton. The impact resistance of composite materials — a review. *Composites 22(5)*, pages 347–362, 1991.

[15] S.W. Case and K.L. Reifsnider. 4.16 - fatigue of composite materials. In I. Milne, R.O. Ritchie, and B. Karihaloo, editors, *Comprehensive Structural Integrity*, pages 405–441. Pergamon, Oxford, 2003.

[16] CBS. Hoeveel personenauto's zijn er in nederland? `https://www.cbs.nl/nl-nl/visualisaties/verkeer-en-vervoer/vervoermiddelen-en-infrastructuur/personenautos`, 2020. [Online; accessed 21-January-2021].

[17] Yu-Chiun Chiou, Chiang Fu, and Chia-Yen Ke. Modelling two-vehicle crash severity by generalized estimating equations. *Accident Analysis and Prevention 148*, page 105841, 2020.

[18] H.Y. Choi, H.-Y.T. Wu, and F.K. Chang. A new approach toward understanding damage mechanisms and mechanics of laminated composites due to low-velocity impact: Part i- experiments. *Journal of Composite Materials 25*, pages 992–1011, 1991.

[19] H.Y. Choi, H.-Y.T. Wu, and F.K. Chang. A new approach toward understanding damage mechanisms and mechanics of laminated composites due to low-velocity impact: Part ii- analysis. *Journal of Composite Materials 25*, pages 1012–1038, 1991.

[20] T.W. Chou, R.L. McCullough, and R.B. Pipes. Composites. *Scientific American 10*, pages 193–203, 1986.

[21] Junjia Cui, Shaoluo Wang, Shuhao Wang, Guangyao Li, Peilin Wang, and Chengsong Liang. The effects of strain rates on mechanical properties and failure behavior of long glass fiber reinforced thermoplastic composites. *Polymers*, 11, 12 2019.

[22] I. De Baere, S. Jacques, W. Van Paepegem, and J. Degrieck. Study of the mode i and mode ii interlaminar behavior of a carbon fabric reinforced tp. *Polym Test, 31(2)*, pages 322–332, 2012.

[23] D. D. Dubey and J. A. Vizzini. Energy absorption of composite plates and tubes. *Composite Materials*, 32:158–176, February 1998.

[24] Ozan Erartsın, Stijn A. J. J. Arntz, Enrico M. Troisi, Leonid V. Pastukhov, Martin van Drongelen, Laurent Warnet, and Leon E. Govaert. Long-term failure of transversely loaded glass/ipp. *Journal of Applied Polymer Science*, 138(35):50878, 2021.

[25] B.G. Falzon, D. Dalli, L.F. Varandas, G. Catalanotti, and S. Foster. Assessing the current modelling approach for predicting the crashworthiness of formula one composite structures. *Composites Part B 201*, page 108242, 2020.

[26] B.G. Falzon and W. Tan. Modelling the crush behaviour of thermoplastic composites. *Composites Science and Technology 134*, pages 57–71, 2016.

[27] K. Friedrich. Fracture mechanical behaviour of short fiber reinforced thermoplastics. *Fortschrittsberichte VDI Zeitschriften, Reihe 18, Nr. 18*, 1984.

[28] K. Friedrich and A.A. Almajid. Manufacturing aspects of advanced polymer composites for automotive applications. *Applied Composite Materials 20*, pages 107–128, 2013.

[29] J Harding and L Mo Welsh. A tensile testing technique for fibre-reinforced composites at impact rates of strain. *Journal of materials science*, 18(6):1810–1826, 1983.

[30] W. Hufenbach, M. Gude, C. Ebert, M. Zscheyge, and A. Hornig. Strain rate dependent low velocity impact response of layerwise 3d-reinforced composite structures. *International Journal of Impact Engineering*, 38(5):358–368, 2011.

[31] D. Hull and T.W. Clyne. *An introduction to composite materials, 2nd edn.* Cambridge University Press, Cambridge, 1996.

[32] Munir Hussain, Feichao Zhu, Bin yu, Jian Han, Hafeezullah Memon, and Sohail Yasin. Lmpp effects on morphology, crystallization, thermal and mechanical properties of ipp/lmpp blend fibres. *Fibres and Textiles in Eastern Europe*, 128, 04 2018.

[33] ASM International and S. Lampman. *Characterization and Failure Analysis of Plastics*. ASM International, 2003.

[34] George C. Jacob, John F. Fellers, Srdan Simunovic, and J. Michael Starbuck. Energy absorption in polymer composites for automotive crashworthiness. *Journal of Composite Materials*, 36(7):813–850, 2002.

[35] B. Z. Jang, D. R. Uhlmann, and J. B. Vander Sande. Crazing in polypropylene. *Polymer Engineering & Science*, 25(2):98–104, 1985. Cited By :41.

[36] G.R. Johnson and W.H. Cook. Fracture characteristics of three metals subjected to various strains, strain rates, temperatures and pressures. *Engineering Fracture Mechanics*, 21(1):358–368, 1985.

[37] Ku-Hyun Jung, Do-Hyoung Kim, Hee-June Kim, Seong-Hyun Park, Kyung-Young Jhang, and Hak-Sung Kim. Finite element analysis of a low-velocity impact test for glass fiber-reinforced polypropylene composites considering mixed-mode interlaminar fracture toughness. *Composite Structures 160*, pages 446–456, 2017.

[38] S. Kalpakjian and S.R. Schmid. *Manufacturing Engineering and Technology*. Prentice Hall international. Prentice Hall, 2001.

[39] Eun-Ho Kim, Mi-Sun Rim, In Lee, and Tae-Kyung Hwang. Composite damage model based on continuum damage mechanics and low velocity impact analysis of composite plates. *Composite Structures 95*, pages 123–134, 2013.

[40] Amit Kumar. Morphology, crystallization and melting behavior of statistical copolymers of propylene with ethylene. Master's thesis, Virginia Polytechnic Institute and State University, 2001.

[41] S.-W.R Lee and C.T. Sun. A quasi-static penetration model for composite laminates. *Journal of Composite Materials 27(3)*, pages 251–271, 1993.

[42] H. Lobo and J. Lorenzo. High speed stress-strain material properties as inputs for the simulation of impact situations. In *IBEC Proceedings*, 1997.

[43] Zakaria Mouti, Keith Westwood, Kambiz Kayvantash, and James Njuguna. Low velocity impact behavior of glass filled fiber-reinforced thermoplastic engine components. *Materials 3*, pages 2463–2473, 2010.

[44] M.R. Nurul Fazita, H.P.S. Abdul Khalil, A. Nor Amira Izzati, and Samsul Rizal. 3 - effects of strain rate on failure mechanisms and energy absorption in polymer composites. In Mohammad Jawaid, Mohamed Thariq, and Naheed Saba, editors, *Failure Analysis in Biocomposites, Fibre-Reinforced Composites and Hybrid Composites*, Woodhead Publishing Series in Composites Science and Engineering, pages 51–78. Woodhead Publishing, 2019.

[45] Michael Okereke, C. Paul Buckley, and Ambrose I. Akpoyomare. The mechanism of rate-dependent off-axis compression of a low fibre volume fraction thermoplastic matrix composite. *Composite Structures*, 168:685–697, 2017.

[46] A Pupurs and J Varna. 3-d FEM modeling of fiber/matrix interface debonding in UD composites including surface effects. *IOP Conference Series: Materials Science and Engineering*, 31:012001, feb 2012.

[47] N Razali, MTH Sultan, F Mustapha, N Yidfris, and MR Ishak. Impact damage on composite structures–a review. *Int. J. Eng. Sci*, 3(7):08–20, 2014.

[48] M.O.W. Richardson and M.J. Wisheart. Review of low velocity impact properties of composite materials. *Composites Part A 27A*, pages 1123–1131, 1996.

[49] J.A Roetling. Yield stress behaviour of isotactic polypropylene. *Polymer*, 7(7):303–306, 1966.

[50] Syafiqah Nur Azrie Bt Safri, M.T.H. Sultan, and Mohammad Jawaid. 7 - damage analysis of glass fiber reinforced composites. In Mohammad Jawaid, Mohamed Thariq, and Naheed Saba, editors, *Durability and Life Prediction in Biocomposites, Fibre-Reinforced Composites and Hybrid Composites*, Woodhead Publishing Series in Composites Science and Engineering, pages 133–147. Woodhead Publishing, 2019.

[51] G. Savage, I. Bomphray, and M. Oxley. Exploiting the fracture properties of carbon fibre composites to design lightweight energy absorbing structures. *Engineering Failure Analysis 11*, pages 677–694, 2004.

[52] C.R. Siviour and J.L. Jordan. High strain rate mechanics of polymers: A review. *Journal of Dynamic Behavior of Materials*, (2):15–32, 2016.

[53] S.W.F. Spronk, M. Kersemans, J.C.A. De Baerdemaeker, F.A. Gilabert, R.D.B. Sevenois, D. Garoz, C. Kassapoglou, and W. Van Paepegem. Comparing damage from low-velocity impact and quasi-static indentation in automotive carbon/epoxy and glass/polyamide-6 laminates. *Polymer Testing 65*, pages 231–241, 2018.

[54] K. Srinivasan, W. C. Jackson, B. T. Smith, and J. A. Hinley. Characterization of damage modes in impacted thermoset and thermoplastic composites. *Reinforced Plastics and Composites Vol 11*, pages 1111–1126, 1992.

[55] G.R. Strobl. *The Physics of Polymers, 1st Edition*. Springer Berlin Heidelberg, 2007.

[56] SWOV. Bestand geregistreerde ongevallen nederland. `https://theseus.swov.nl/single/?appid=d1569e91-8a56-4922-a336-2373764a6889&sheet=PfWALm&opt=currsel%2Cctxmenu`, 2020. [Online; accessed 21-January-2021].

[57] R. Talreja. 2 - a mechanisms-based framework for describing failure in composite materials. In P.W.R. Beaumont, C. Soutis, and A. Hodzic, editors, *Structural Integrity and Durability of Advanced Composites*, Woodhead Publishing Series in Composites Science and Engineering, pages 25–42. Woodhead Publishing, 2015.

[58] G. Trantina and P. Oehler. Standardization, is it leading to more relevant data for design engineers? In *SPE ANTEC Proceedings*, 1994.

[59] Himayat Ullah and Vadim V. Silberschmidt. Numerical analysis of the interactive damage mechanisms in two-dimensional carbon fabric-reinforced thermoplastic composites under low velocity impacts. *Journal of Composite Materials 49 (25)*, pages 3127–3143, 2014.

[60] C. Untaroiu and Y. Meng. Numerical investigation of occupant injury risks in car-to-end terminal crashes using dummy-based injury criteria and vehicle-based crash severity metrics. *Accident Analysis and Prevention 145*, page 105700, 2020.

[61] A.K. van der Vegt and L.E. Govaert. *Polymeren: van keten tot kunststof*. VSSD, 2005.

[62] B. Vieille, J.-D. Pujols-Gonzalez, C. Bouvet, T. Breteau, and C. Gautrelet. Influence of impact velocity on impact behaviour of hybrid woven-fibers reinforced peek thermoplastic laminates. *Composite Part C*, 2020.

[63] SM Walley and JE Field. Strain rate sensitivity of polymers in compression from low to high rates. *DYMAT j*, 1(3):211–227, 1994.

[64] J. G. Williams and G. C. Adams. The analysis of instrumented impact tests using a mass-spring model. *International Journal of Fracture*, 33(3):209–222, 1987.

[65] Lei Yang, Zhanjun Wu, Dongyue Gao, and Xin Liu. Microscopic damage mechanisms of fibre reinforced composite laminates subjected to low velocity impact. *Computational Materials Science*, 111:148–156, 2016.

[66] S.M Zebarjad, R Bagheri, A Lazzeri, and S Serajzadeh. Fracture behaviour of isotactic polypropylene under static loading condition. *Materials & Design*, 24(2):105–109, 2003.

[67] D. Zeleniakiene, P. Griskevicius, A. Aniskevich, V. Jankauskaite, and K. Zukiene. A numerical and experimental study on the impact behavior of a carbon-fiber-reinforced thermoplastic poly (methyl methacrylate) composite. *Mechanics of Composite Materials Vol 55, No 3*, pages 393–404, 2019.

[68] Q. Zeng, H. Huang, and C. Li. Crash protectiveness to occupant injury and vehicle damage: An investigation on major car brands. *Accident Analysis and Prevention 86*, pages 129–136, 2016.

[69] C. Zweben, W. Smith, and M. Wardle. Test methods for fiber tensile strength, composite flexural modulus, and properties of fabric-reinforced laminates. Standard, ASTM International, West Conshohocken, PA, 1979.

Appendix A

Specimen Data

A.1 90° Specimens

Table A.1: Quasi-Static Three Point Bending at room temperature

Sample ID	Thickness [mm]	Width [mm]	Length [mm]
61	1,94	11,59	60,49
62	1,91	11,79	59,19
63	1,91	11,92	59,07
64	1,93	11,80	60,72
65	1,92	11,63	59,53
71	1,96	11,61	60,01
72	1,92	11,72	60,49
73	1,95	11,48	60,27
74	1,95	11,47	59,35
75	1,92	11,51	59,47
81	1,90	11,67	60,25
82	1,91	11,76	59,47
83	1,96	11,50	60,05
84	1,89	11,79	60,59
85	1,91	11,71	60,18

Table A.2: Low Velocity Drop Weight Impact

Sample ID	Thickness [mm]	Width [mm]	Length [mm]
101	1,96	11,61	60,36
102	1,90	11,87	59,75
103	1,92	11,98	59,57
104	1,94	11,87	60,08
105	1,95	11,51	59,08
106	1,90	11,75	59,65
107	1,98	11,73	60,88
108	1,92	11,99	60,53
109	1,94	11,58	59,51
111	1,92	11,63	59,91
112	1,91	11,68	60,29
113	1,91	11,89	60,17
114	1,92	11,55	60,29
115	1,99	11,69	59,57
116	1,96	11,89	60,94
117	1,93	11,91	60,55
118	1,95	11,66	59,01
119	1,94	11,76	59,85

Table A.3: Quasi-Static Three Point Bending at different Temperatures

Sample ID	Thickness [mm]	Width [mm]	Length [mm]
91	1,98	11,55	60,64
92	1,96	11,83	60,56
93	1,89	11,64	59,82
94	1,94	11,65	59,40
95	1,89	11,78	60,89
86	1,95	11,49	59,92
87	1,94	11,08	60,09
88	1,92	11,81	60,04
89	1,91	11,85	59,34
96	1,92	12,08	59,10
97	1,93	11,72	59,05
98	1,96	11,41	60,26
99	1,97	11,74	59,23

A.2 0° Specimens

Table A.4: Quasi-Static Three Point Bending at room temperature

Sample ID	Thickness [mm]	Width [mm]	Length [mm]
61	1,91	11,54	60,31
62	1,96	11,71	60,57
63	1,90	11,53	59,25
64	1,88	11,66	60,72
65	1,87	11,64	59,31
71	1,94	11,74	59,01
72	1,95	11,80	60,15
73	1,93	11,74	60,58
74	1,91	11,60	59,74
75	1,86	11,71	59,73
81	1,93	11,78	59,81
82	1,88	11,70	59,68
83	1,92	11,56	60,14
84	1,95	11,76	59,65
85	1,94	11,74	60,46

Table A.5: Low Velocity Drop Weight Impact

Sample ID	Thickness [mm]	Width [mm]	Length [mm]
101	1,94	11,53	60,61
102	1,96	11,24	60,39
103	1,95	11,70	60,35
104	1,92	11,70	59,04
105	1,92	11,70	60,10
106	1,93	11,68	60,14
107	1,95	11,60	60,36
108	1,94	11,71	60,67
109	1,94	11,65	60,50
110	1,87	11,66	58,29
111	1,95	11,28	60,36
112	1,86	11,62	60,95
113	1,92	11,68	59,75
114	1,94	11,70	60,53
115	1,86	11,65	59,99
116	1,87	11,58	58,84

Table A.6: Quasi-Static Three Point Bending at different Temperatures

Sample ID	Thickness [mm]	Width [mm]	Length [mm]
91	1,96	11,77	59,94
92	1,93	11,78	60,18
93	1,96	11,82	59,90
94	1,94	11,67	60,71
95	1,91	11,62	59,87
86	1,90	11,05	60,08
87	1,90	11,46	60,28
88	1,89	11,63	59,57
89	1,88	11,69	59,25
96	1,92	11,65	60,73
97	1,96	11,44	60,95
98	1,90	11,69	60,92
99	1,93	11,65	60,95

Appendix B

Force-Displacement Plots LVI

B.1 90° Specimens

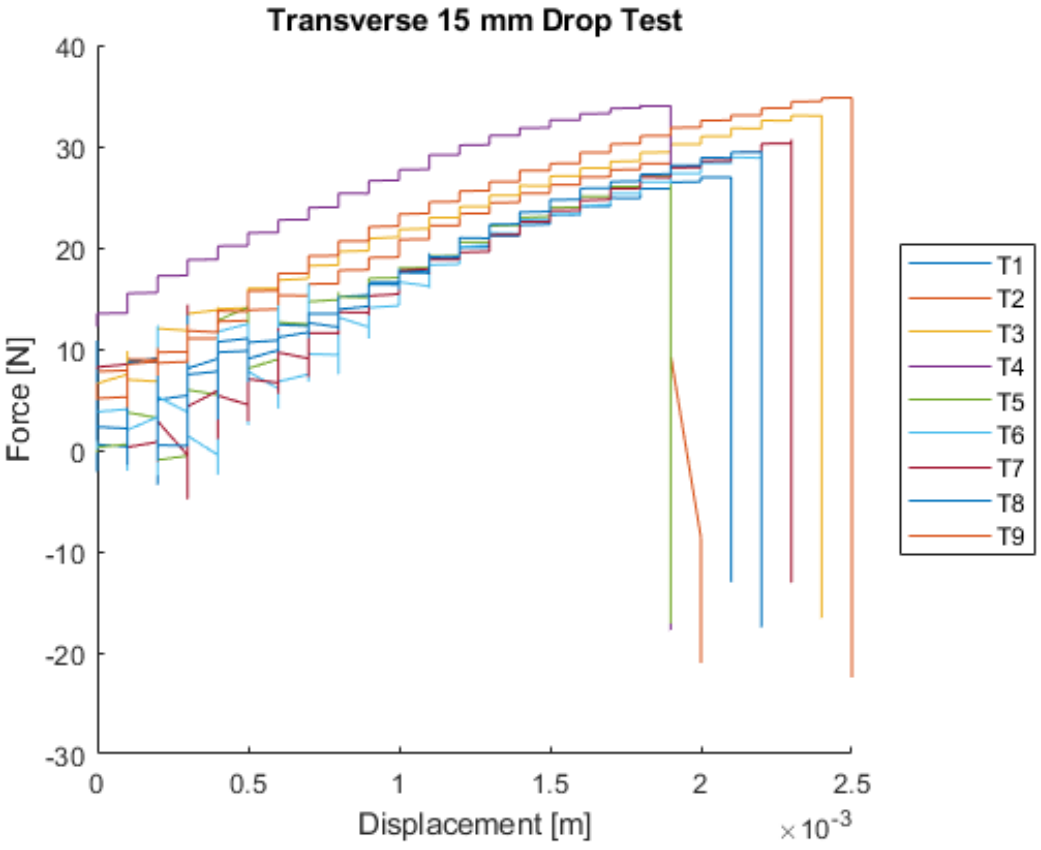

Figure B.1: Force-Displacement curve of 90° specimens under 0.23 J impact energy

B.2 0° Specimens

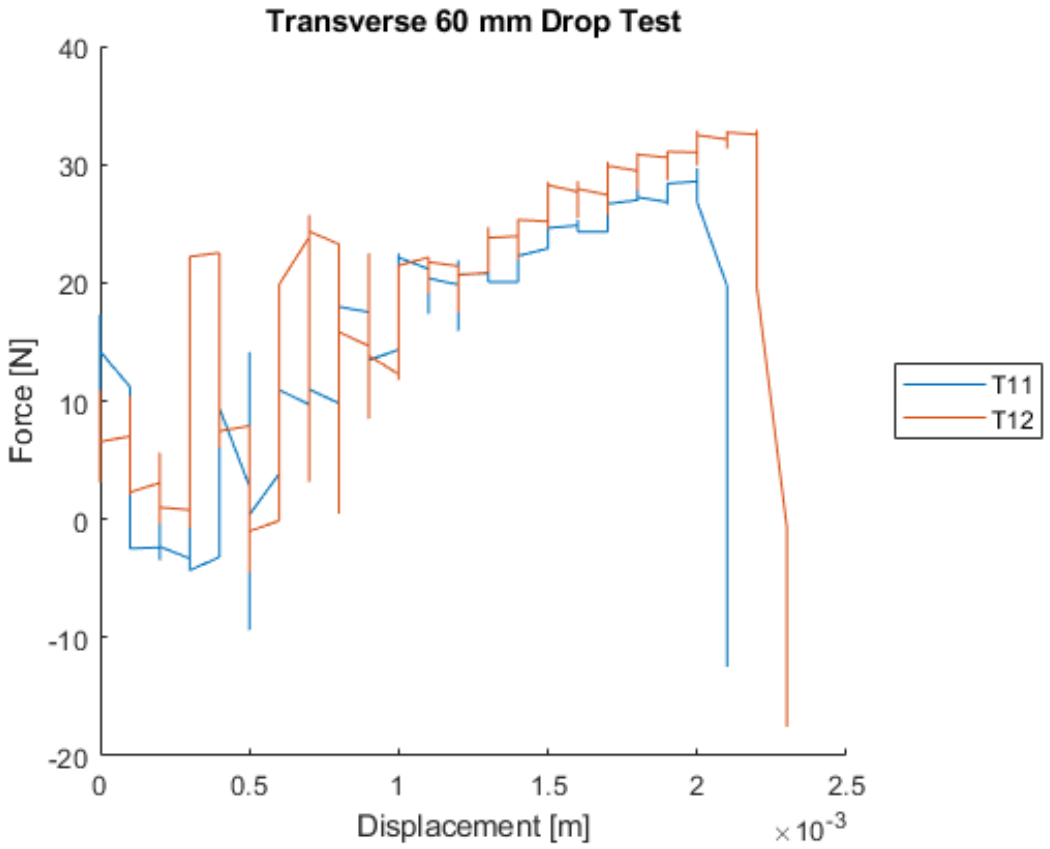

Figure B.2: Force-Displacement curve of 90° specimens under 0.93 J impact energy

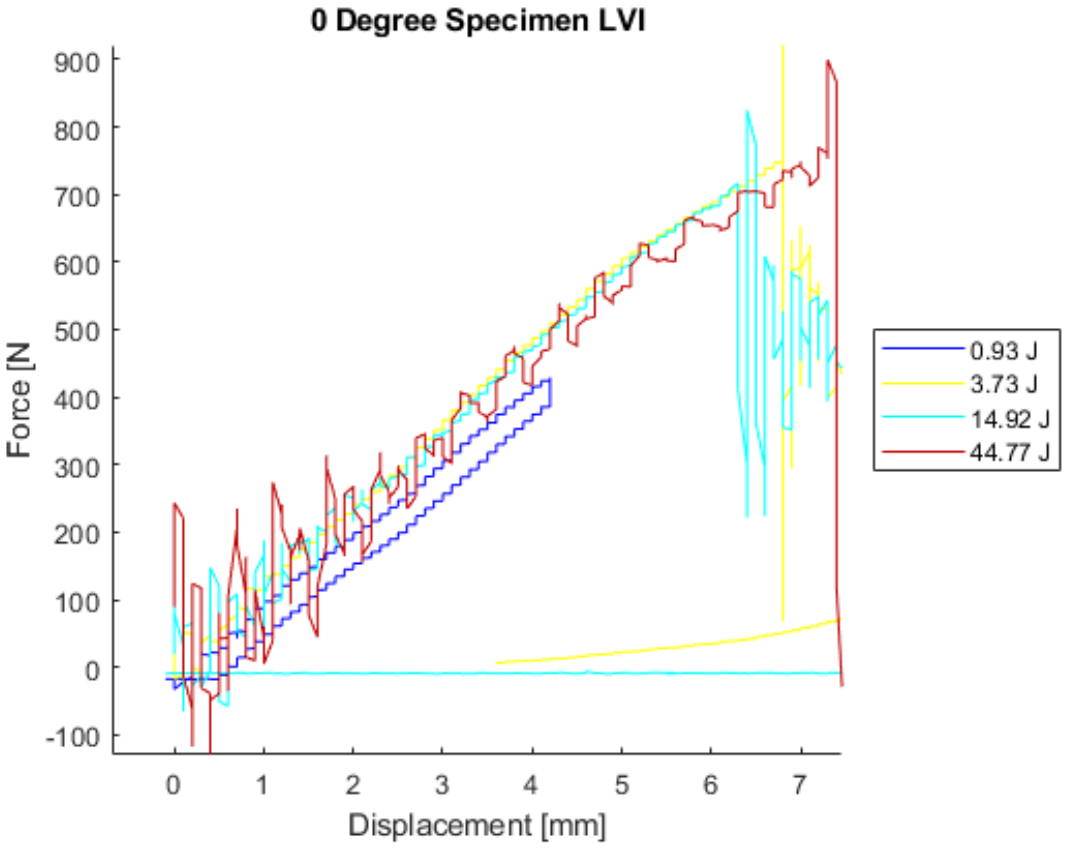

Figure B.3: Force-Displacement curve of 0° specimens